Contents

Chapter 27

Gravitational Waves and Experimental Tests of General Relativity

Version 1327.1.K.pdf, 30 January 2014.

Box 27.1
Reader's Guide

- This chapter relies significantly on
  - Chapter 2 on special relativity
  - Chapter 24, on the transition from special relativity to general relativity.
  - Chapter 25, on the fundamental concepts of general relativity, especially Sec. 25.9 on weak, relativistic gravitational fields.
  - Chapter 26, on relativistic stars and black holes.
  - Sec. 7.3 on geometric optics.
- In addition, Sec. 27.2.3 on Fermat's principle and gravitational lenses is closely linked to Sec. 7.6 on gravitational lenses and Sec. 8.6 on diffraction at a caustic.
- Portions of this chapter are a foundation for Chap. 28, Cosmology.

27.1 Overview

In 1915, when Einstein formulated general relativity, human technology was incapable of definitive experimental tests of his theory. Only a half century later did technology begin to catch up. In the years since then, the best experiments have improved from accuracies of a few tens of per cent to a part in 10,000 or 100,000; and general relativity has passed the tests with flying colors. In Sec. 27.2, we shall describe some of these tests, derive general relativity's predictions for them, and discuss the experimental results.

In the near future, observations of gravitational waves will radically change the character of research on general relativity. They will produce, for the first time, tests of general relativity in strong-gravity situations. They will permit us to study relativistic effects in neutron-star and black-hole binaries with exquisite accuracies. They will enable us to map the spacetime geometries of black holes with high precision, and study observationally the large-amplitude, highly nonlinear vibrations of curved spacetime that occur when two black holes collide and merge. And (as we shall see in Chap. 28), they may enable us to probe the singularity in which the universe was born and the universe's evolution in its first tiny fraction of a second.

In this chapter, we shall develop the theory of gravitational waves in much detail and shall describe the efforts to detect the waves and the sources that may be seen. More specifically, in Sec. 27.3, we shall develop the mathematical description of gravitational waves, both classically and quantum mechanically (in the language of gravitons), and we shall study their propagation through flat spacetime. Then, in Sec. 27.4, we shall study their propagation through curved spacetime using the tools of geometric optics. In Sec. 27.5, we shall develop the simplest approximate method for computing the generation of gravitational waves, the "quadrupole-moment formalism"; and we shall describe and present a few details of other, more sophisticated and accurate methods based on multipolar expansions, post-Newtonian techniques, and numerical simulations on supercomputers ("numerical relativity"). In Sec. 27.6, we shall turn to gravitational-wave detection, focusing especially on detectors such as LIGO and LISA that rely on laser interferometry.

27.2 Experimental Tests of General Relativity

In this section, we shall describe briefly some of the most important experimental tests of general relativity. For greater detail and other tests, see Will (1993ab, 2001, 2006)

27.2.1 Equivalence Principle, Gravitational redshift, and Global Positioning System

A key aspect of the equivalence principle is the prediction that any object, whose size is extremely small compared to the radius of curvature of spacetime and on which no nongravitational forces act, should move on a geodesic. This means, in particular, that its trajectory through spacetime should be independent of its chemical composition. This is called the *weak equivalence principle*, or the *universality of free fall*.

Efforts to test the universality of free fall date back to Galileo's (perhaps apocryphal) experiment of dropping objects from the leaning tower of Pisa. Over the past century, a sequence of ever-improving experiments led by Roland von Eötvös ($\sim$ 1920), Robert Dicke ($\sim$ 1964), Vladimir Braginsky ($\sim$ 1972), and Eric Adelberger ($\sim$ 2008) have led to an accuracy $\Delta a/a < 2 \times 10^{-13}$ for the difference of gravitational acceleration toward the sun for earth-bound bodies with very different chemical composition (Schlamminger et. al. 2008). A proposed space experiment called *STEP* has the prospect to increase this accuracy to the phenomenal level of $\Delta a/a \lesssim 1 \times 10^{-18}$.

General relativity predicts that bodies with significant self gravity (even black holes) should also fall, in a nearly homogeneous external gravitational field, with the same acceleration as a body with negligible self gravity. This prediction has been tested by comparing the gravitational accelerations of the earth and moon toward the sun. Their fractional difference of acceleration [as determined by tracking the relative motions of the moon and earth using laser beams fired from earth, reflected off mirrors that astronauts and cosmonauts have placed on the moon, and received back at earth] has been measured to be $\Delta a/a \lesssim 1 \times 10^{-13}$. Since the earth and moon have (gravitational potential energy)/(rest-mass energy) $\simeq -4 \times 10^{-10}$ and $\simeq -2 \times 10^{-11}$ respectively, this verifies that gravitational energy falls with the same acceleration as other forms of energy to within about 2.5 parts in 10,000. For references and for discussions of a variety of other tests of the Equivalence Principle, see Merkowitz (2010) and Will (1993b, 2005).

From the equivalence principle, one can deduce that, for an emitter and absorber at rest in a Newtonian gravitational field Φ, light (or other electromagnetic waves) must be gravitationally redshifted by an amount $\Delta\lambda/\lambda = \Delta\Phi$, where $\Delta\Phi$ is the difference in Newtonian potential between the locations of the emitter and receiver. (See Ex. 26.4 for a general relativistic derivation when the field is that of a nonspinning, spherical central body with the emitter on the body's surface and the receiver far from the body; see Ex. 24.16 for a derivation when the emitter and receiver are on the floor and celing of an earth-bound laboratory.) Relativistic effects will produce a correction to this shift with magnitude $\sim (\Delta\Phi)^2$ [cf. Eq. (26.18)], but for experiments performed in the solar system, the currently available precision is too poor to see this correction, so such experiments test the equivalence principle and not the details of general relativity.

The highest precision test of this gravitational redshift thus far was NASA's 1976 Gravity-Probe-A Project (led by Robert Vessot), in which several atomic clocks were flown to a height of about 10,000 km above the earth, and were compared with atomic clocks on the earth via radio signals transmitted downward. After correcting for special relativistic effects due to the relative motions of the rocket's clocks and the earth clocks, the measured gravitational redshift agreed with the prediction to within the experimental accuracy of about 2 parts in 10,000.

The Global Positioning System (GPS), by which one can routinely determine one's location on earth to within an accuracy of about 10 meters, is based on signals transmitted from a set of earth-orbiting satellites. Each satellite's position is encoded on its transmitted signals, together with the time of transmission as measured by atomic clocks onboard the satellite. A person's GPS receiver contains a high-accuracy clock and a computer. It measures the signal arrival time and compares with the encoded transmission time to determine the distance from satellite to receiver; and it uses that distance, for several satellites, together with the encoded satellite positions, to determine (by triangulation) the receiver's location on earth.

The transmission times encoded on the signals are corrected for the gravitational redshift before transmission. Without this redshift correction, the satellite clocks would quickly get out of synchronization with all the clocks on the ground, thereby eroding the GPS accuracy; see Ex. 27.1. Thus, a good understanding of general relativity was crucial to the design of the GPS!

****

EXERCISES

Exercise 27.1 *Practice: Gravitational Redshift for Global Positioning System*
The GPS satellites are in circular orbits at a height of 20,200 km above the earth's surface, where their orbital period is 12 sidereal hours. If the ticking rates of the clocks on the satellites were not corrected for the gravitational redshift, roughly how long would it take them to accumulate a time shift, relative to clocks on the earth, large enough to degrade the GPS position accuracy by 10 meters? by 1 kilometer?

****

27.2.2 Perihelion Advance of Mercury

It was known at the end of the nineteenth century that the point in Mercury's orbit closest to the sun, known as its perihelion, advances at a rate of about $575''$ per century with respect to the fixed stars, of which about $532''$ can be accounted for by Newtonian perturbations due to the other planets. The remaining $\sim 43''$ per century was a mystery until Einstein showed that it can be accounted for quantitatively by the general theory of relativity.

More specifically (as is demonstrated in Ex. 27.2), if we idealize the sun as nonrotating and spherical so its external gravitational field is Schwarzschild, and we ignore the presence of the other planets, and we note that the radius of Mercury's orbit is very large compared to the sun's mass (in geometrized units), then Mercury's orbit will be very nearly an ellipse; and the ellipse's perihelion will advance, from one orbit to the next, by an angle

$$\boxed{\Delta\phi = 6\pi M/p + \mathcal{O}(M^2/p^2) \quad \text{radians}} \,. \tag{27.1}$$

Here M is the sun's mass and p is the ellipse's *semi latus rectum*, which is related to its semimajor axis a (half its major diameter) and its eccentricity e by $p = a(1-e^2)$. For the parameters of Mercury's orbit ($M = M_\odot \simeq 1.4766$ km, $a = 5.79089 \times 10^7$ km, $e = 0.205628$), this advance is $0.10352''$ per orbit. Since the orbital period is 0.24085 earth years, this advance corresponds to 42.98 arc seconds per century.

Although the sun is not precisely spherical, its tiny gravitational oblateness (as inferred from measurements of its spectrum of pulsations; Fig. 16.3) has been shown to contribute negligibly to this perihelion advance; and the frame dragging due to the sun's rotational angular momentum is also (sadly!) negligible compared to the experimental accuracy; so $42.98''$ per century is the relativistic contribution to Mercury's perihelion advance. Modern observational data agree with this to within the data's accuracy of about 1 part in 1000.

****

EXERCISES

Exercise 27.2 *Example: Perihelion Advance*

Consider a small satellite in non-circular orbit about a spherical body with much larger mass M, for which the external gravitational field is Schwarzschild. The satellite will follow a timelike geodesic. Orient the Schwarzschild coordinates so the satellite's orbit is in the equatorial plane, $\theta = \pi/2$.

(a) Because the metric coefficients are independent of t and ϕ, the satellite's energy-at-infinity $\mathcal{E}_\infty = -p_t$ and angular momentum $L = p_\phi$ must be constants of the satellite's motion (Ex. 25.4). Show that

$$\mathcal{E}_\infty = \left(1 - \frac{2M}{r}\right)\frac{dt}{d\tau}\,, \quad L = r^2\frac{d\phi}{d\tau}\,. \tag{27.2a}$$

See Ex. 26.12. Here and below we take the satellite to have unit mass, so its momentum and 4-velocity are the same and its affine parameter ζ and proper time τ are the same.

(b) Introduce the coordinate $u = r^{-1}$ and use the normalization of the 4-velocity to derive the following differential equation for the orbit:

$$\left(\frac{du}{d\phi}\right)^2 = \frac{\mathcal{E}_\infty^2}{L^2} - \left(u^2 + \frac{1}{L^2}\right)(1 - 2Mu)\,. \tag{27.2b}$$

(c) Differentiate this equation with respect to ϕ to obtain a second order differential equation

$$\frac{d^2u}{d\phi^2} + u - \frac{M}{L^2} = 3Mu^2. \tag{27.2c}$$

By reinstating the constants G, c, and comparing with the Newtonian orbital equation, argue that the right-hand side represents a relativistic perturbation to the Newtonian equation of motion.

(d) Assume, henceforth in this exercise, that $r \gg M$ (i.e. $u \ll 1/M$), and solve the orbital equation (27.2c) by perturbation theory. More specifically: At zero order (i.e., setting the right side to zero), show that the Kepler ellipse

$$u_K = \left(\frac{M}{L^2}\right)(1 + e\cos\phi), \tag{27.2d}$$

is a solution. Here e (a constant of integration) is the ellipse's eccentricity and L^2/M is the ellipse's *semi latus rectum*. The orbit has its minimum radius at $\phi = 0$.

(e) By substituting u_K into the right hand side of the relativistic equation of motion (27.2c), show (at first-order in the relativistic perturbation) that in one orbit the angle ϕ at which the satellite is closest to the mass advances by $\Delta\phi \simeq 6\pi M^2/L^2$. (Hint: Try to write the differential equation in the form $d^2u/d\phi^2 + (1+\epsilon)^2 u \simeq \ldots$, where $\epsilon \ll 1$.)

(f) For the planet Mercury, the orbital period is $P = 0.241$ yr and the eccentricity is $e = 0.206$. Deduce that the relativistic contribution to the rate of advance of the *perihelion* (point of closest approach to the sun) is $43''$ per century.

Exercise 27.3 *Example: Gravitational Deflection of Light.*
Repeat the analysis of Ex. 27.2 for a photon following a null geodesic. More specifically:

(a) Show that the photon trajectory $u(\phi)$ (with $u \equiv 1/r$) obeys the differential equation

$$\frac{d^2u}{d\phi^2} + u = 3Mu^2 \ . \tag{27.3}$$

(b) Obtain the zero'th order solution by ignoring the right hand side,

$$u = \frac{\sin\phi}{b} \ . \tag{27.4}$$

where b is an integration constant. Show that this is just a straight line in the asymptotically flat region far from the body, and b is the impact parameter (projected distance of closest approach to the body).

(c) Substitute this solution into the right hand side and show that the perturbed trajectory satisfies

$$u = \frac{\sin\phi}{b} + \frac{M}{b^2}(1-\cos\phi)^2 \ . \tag{27.5}$$

(d) Hence show that a ray with impact parameter $b \gg M$ will be deflected through an angle

$$\alpha = \frac{4M}{b} \ ; \tag{27.6}$$

cf. Eq. (6.77) and associated discussion.

****

27.2.3 Gravitational Deflection of Light, Fermat's Principle and Gravitational Lenses

Einstein not only explained the anomalous perihelion shift of Mercury. He also predicted (Ex. 27.3) that the null rays along which starlight propagates will be deflected, when passing through the curved spacetime near the sun, by an angle

$$\boxed{\Delta\phi = 4M/b + \mathcal{O}(M^2/b^2)} \ , \tag{27.7}$$

relative to their trajectories if spacetime were flat. Here M is the sun's mass and b is the ray's impact parameter (distance of closest approach to the sun's center). For comparison, theories that incorporated a Newtonian-like gravitational field into special relativity (Sec 25.1 and Ex. 25.1) predicted no deflection of light rays; and the corpuscular theory of light combined with Newtonian gravity predicted half the general relativistic deflection, as did a 1911 principle-of-equivalence argument by Einstein that was ignorant of the curvature of space. The deflection was measured to an accuracy ~ 20 per cent during the 1919 solar eclipse and agreed with

general relativity rather than the competing theories—a triumph that helped make Einstein famous. Modern experiments, based on the deflection of radio waves from distant quasars, as measured using Very Long Baseline Interferometry (interfering the waves arriving at radio telescopes with transcontinental or transworld separations; Sec. 9.3), have achieved accuracies of about 1 part in 10,000, and they agree completely with general relativity. Similar accuracies are now achievable using optical interferometers in space, and may soon be achievable via optical interferometry on the ground.

These accuracies are so great that, when astronomers make maps of the sky using either radio interferometers or optical interferometers, they must now correct for gravitational deflection of the rays *not only when the rays pass near the sun, but for rays coming in from nearly all directions*. This correction is not quite as easy as Eq. (27.7) suggests, since that equation is valid only when the telescope is much farther from the sun than the impact parameter. In the more general case, the correction is more complicated, and must include aberration due to the telescope motion as well as the effects of spacetime curvature.

The gravitational deflection of light rays passing through or near a cluster of galaxies can produce a spectacular array of distorted images of the light source. In Sec. 7.6, we deduced the details of this *gravitational lens effect* using a model in which we treated spacetime as flat, but endowed with a refractive index $\mathfrak{n}(\mathbf{x}) = 1 - 2\Phi(\mathbf{x})$, where $\Phi(\mathbf{x})$ is the Newtonian gravitational potential of the lensing system. This model can also be used to compute light deflection in the solar system. We shall now derive this model from general relativity.

The foundation for this model is the following general relativistic version of *Fermat's principle* [see Eq. (7.45) for the Newtonian version]: *Consider any static spacetime geometry,* i.e. one for which we can introduce a coordinate system in which $\partial g_{\alpha\beta}/\partial t = 0$ and $g_{jt} = 0$; so the only nonzero metric coefficients are $g_{00}(x^k)$ and $g_{ij}(x^k)$. In such a spacetime the time coordinate t is very special, since it is tied to the spacetime's temporal symmetry. An example is Schwarzschild spacetime and the Schwarzschild time coordinate t. Now, consider a light ray emitted from a spatial point $x^j = a^j$ in the static spacetime and received at a spatial point $x^j = b^j$. Assuming the spatial path along which the ray travels is $x^j(\eta)$, where η is any parameter with $x^j(0) = a^j$, $x^j(1) = b^j$, then the total coordinate time Δt required for the light's trip from a^j to b^j (as computed from the fact that the ray must be null so $ds^2 = g_{00}dt^2 + g_{ij}dx^i dx^j = 0$) is

$$\boxed{\Delta t = \int_0^1 \sqrt{\gamma_{jk}\frac{dx^j}{d\eta}\frac{dx^k}{d\eta}}d\eta\ , \quad \text{where} \quad \gamma_{jk} \equiv \frac{g_{jk}}{-g_{00}}}\ . \tag{27.8}$$

Fermat's principle says that *the actual spatial trajectory of the light path, in any static spacetime, is one that extremizes this coordinate time lapse.*

This principle can be proved (Ex. 27.4) by showing that the Euler-Lagrange equation for the action (27.8) is equivalent to the geodesic equation for a photon in the static spacetime with metric $g_{\mu\nu}(x^k)$.

The index-of-refraction formalism used to study gravitational lenses in Chap. 7 is easily deduced as a special case of this Fermat principle: In a nearly Newtonian situation, the linearized-theory, Lorenz-gauge, trace-reversed metric perturbation has the form (25.91) with only the time-time component being significantly large: $\bar{h}_{00} = -4\Phi$, $\bar{h}_{0j} \simeq 0$, $\bar{h}_{jk} \simeq 0$.

Correspondingly, the metric perturbation [obtained by inverting Eq. (25.85)] is $h_{00} = -2\Phi$, $h_{jk} = -\delta_{jk}\Phi$, and the full spacetime metric $g_{\mu\nu} = \eta_{\mu\nu} + h_{\mu\nu}$ is

$$ds^2 = -(1+2\Phi)dt^2 + (1-2\Phi)\delta_{jk}dx^j dx^k \ . \tag{27.9}$$

This is the standard spacetime metric (25.79) in the Newtonian limit, with a special choice of spatial coordinates, those of linearized-theory Lorenz gauge. The Newtonian limit includes the slow-motion constraint that time derivatives of the metric are small compared to spatial derivatives [Eq. (25.75b)], so on the timescale for light to travel through a lensing system, the Newtonian potential can be regarded as static, $\Phi = \Phi(x^j)$. Therefore the Newtonian-limit metric (27.9) can be regarded as static, and the coordinate time lapse along a trajectory between two spatial points, Eq. (27.8), reduces to

$$\Delta t = \int_0^1 (1-2\Phi)d\ell \ , \tag{27.10}$$

where $d\ell = \sqrt{\delta_{jk}dx^j dx^k}$ is distance traveled treating the coordinates as though they were Cartesian, in flat space. According to the relativistic Fermat principle (27.8), this Δt is extremal for light rays. However, Eq. (27.10) is also the action for the Newtonian, nongravitational version of Fermat's principle, Eq. (6.42), with index of refraction

$$\boxed{\mathfrak{n}(x^j) = 1 - 2\Phi(x^j)} \ . \tag{27.11}$$

Therefore, the spatial trajectories of the light rays can be computed via the Newtonian Fermat principle, with the index of refraction (27.11). *QED*

Although this index-of-refraction model involves treating a special (Lorenz-gauge) coordinate system as though the spatial coordinates were Cartesian and space were flat (so $d\ell^2 = \delta_{jk}dx^j dx^k$)— which does not correspond to reality—, nevertheless, this model predicts the correct gravitational lens images. The reason is that it predicts the correct rays through the Lorenz-gauge coordinates, and when the light reaches earth, the cumulative lensing has become so great that the fact that the coordinates here are slightly different from truly Cartesian has negligible influence on the images one sees.

****

EXERCISES

Exercise 27.4 *Derivation: Fermat's Principle for a Photon's Path in a Static Spacetime*
Show that the Euler-Lagrange equation for the action principle (27.8) is equivalent to the geodesic equation for a photon in the static spacetime metric $g_{00}(x^k)$, $g_{ij}(x^k)$. Specifically:

(a) The action (27.8) is the same as that for a geodesic in a 3-dimensional space with metric γ_{jk} and with t playing the role of proper distance traveled [Eq. (25.19) converted to a positive-definite, three-dimensional metric]. Therefore, the Euler-Lagrange equation for (27.8) is the geodesic equation in that (fictitious) space [Eq. (25.14) with t the affine parameter.] Using Eq. (24.38c) for the connection coefficients, show that the the geodesic equation can be written in the form

$$\gamma_{jk}\frac{d^2x^k}{dt^2} + \frac{1}{2}(\gamma_{jk,l} + \gamma_{jl,k} - \gamma_{kl,j})\frac{dx^k}{dt}\frac{dx^j}{dt} = 0 \ . \tag{27.12a}$$

(b) Take the geodesic equation (25.14) for the light ray in the real spacetime, with spacetime affine parameter ζ, and change parameters to t. Thereby obtain

$$g_{jk}\frac{d^2x^k}{dt^2} + \Gamma_{jkl}\frac{dx^k}{dt}\frac{dx^l}{dt} - \Gamma_{j00}\frac{g_{kl}}{g_{00}}\frac{dx^k}{dt}\frac{dx^l}{dt} + \frac{d^2t d\zeta^2}{(dt/d\zeta)^2}g_{jk}\frac{dx^k}{dt} = 0 \ ,$$
$$\frac{d^2t/d\zeta^2}{(dt/d\zeta)^2} + 2\Gamma_{0k0}\frac{dx^k/dt}{g_{00}} = 0 \ . \qquad (27.12b)$$

(c) Insert the second of these equations into the first and write the connection coefficients in terms of derivatives of the spacetime metric. With a little algebra, bring your result into the form (27.12a) of the Fermat-principle Euler equation.

****

27.2.4 Shapiro time delay

In 1964, Irwin Shapiro proposed a new experiment to test general relativity: Monitor the round-trip travel time for radio waves transmitted from earth and bounced off Venus or some other planet, or transponded by a spacecraft. As the line-of-sight between the earth and the planet or spacecraft gradually moves nearer then farther from the sun, the waves' rays will pass through regions of greater then smaller spacetime curvature, and this will influence the round-trip travel time by greater then smaller amounts. From the time evolution of the round-trip time, one can deduce the changing influence of the sun's spacetime curvature.

One can compute the round-trip travel time with the aid of Fermat's (geometric-optics) principle. The round-trip proper time, as measured on earth (neglecting, for simplicity, the earth's orbital motion; i.e., pretending the earth is at rest relative to the sun while a radio-wave's rays go out and back) is $\Delta\tau_\oplus = \sqrt{1-2M/r_\oplus}\ \Delta t \simeq (1 - M/r_\oplus)\Delta t$, where M is the sun's mass, $r_\oplus$ is the earth's distance from the sun's center, Δt is the round-trip coordinate time in the static solar-system coordinates, and we have used $g_{00} = -(1-2M/r_\oplus)$ at earth. Because Δt obeys Fermat's principle, it is stationary under small perturbations of the ray's spatial trajectory. This allows us to compute it using a straight-line trajectory through the spatial coordinate system. Letting b be the impact parameter (the ray's closest coordinate distance to the sun) and ℓ be coordinate distance along the straight-line trajectory and neglecting the gravitational fields of the planets, we have $\Phi = -M/\sqrt{\ell^2+b^2}$, so the coordinate time lapse out and back is [Eq. (27.10)]

$$\Delta t = 2\int_{-\sqrt{r_\oplus^2-b^2}}^{\sqrt{r_{\rm refl}^2-b^2}} \left(1 + \frac{2M}{\sqrt{\ell^2+b^2}}\right) d\ell \ . \qquad (27.13)$$

Here $r_{\rm refl}$ is the radius of the location at which the ray gets reflected (or transponded) back to earth. Performing the integral and multiplying by $\sqrt{g_{00}} \simeq 1 - M/r_\oplus$, we obtain for the round-trip travel time measured on earth

$$\Delta\tau_\oplus = 2\,(a_\oplus + a_{\rm refl})\left(1 - \frac{M}{r_\oplus}\right) + 4M\ln\left[\frac{(a_\oplus + r_\oplus)(a_{\rm refl} + r_{\rm refl})}{b^2}\right] \ , \qquad (27.14)$$

where $a_\oplus = \sqrt{r_\oplus^2 - b^2}$ and $a_{\rm refl} = \sqrt{r_{\rm refl}^2 - b^2}$.

As the earth and the reflecting planet or transponding spacecraft move along their orbits, only one term in this round-trip time varies sharply: the term

$$\boxed{\Delta\tau_\oplus = 4M\ln(1/b^2) = -8M\ln b \simeq -40\mu{\rm s}\ \ln b}\ . \tag{27.15}$$

When the planet or spacecraft passes nearly behind the sun, as seen from earth, b plunges to a minimum (on a timescale of hours or days) then rises back up, and correspondingly the time delay shows a sharp blip. By comparing the observed blip with the theory in a measurement with the Cassini spacecraft, this Shapiro time delay has been verified to the remarkable precision of about 1 part in 100,000 (Bertotti, Iess and Tortora 2003).

27.2.5 Frame Dragging, Gravity Probe B, and LAGEOS

As we have discussed in Secs. 25.9.3 and 26.5, the angular momentum $\mathbf{J}$ of a gravitating body places its imprint on the body's asymptotic spacetime metric

$$ds^2 = -\left(1 - \frac{2M}{r}\right)dt^2 - \frac{4\epsilon_{jkm}J^k x^m}{r^3}dt\,dx^j + \left(1 + \frac{2M}{r}\right)\delta_{jk}dx^j dx^k\ . \tag{27.16}$$

[Eq. (25.98c)], and that imprint can be measured by the frame-dragging precession it induces in gyroscopes [Eq. (25.100)].

In magnitude, the precessional angular velocity is $\Omega \sim J/r^3 \sim$(one arcsec per century) in the vicinity of earth, due to the earth's spin angular momentum; so measuring it is a tough experimental challenge. Remarkably, this frame-dragging has been measured successfully, confirming the prediction to approximately 20 percent accuracy, in two ways: by a set of superconducting gyroscopes in earth orbit (the Gravity-Probe B experiment, Everitt et.al. 2011) and by the observations of two very compact, heavy earth-orbiting satellites whose orbital motions act like gyroscopes (the LAGEOS satellites, Ciufolini et. al. 2011 and papers cited therein).[1] Frame dragging has also been seen in distant astronomical objects, but not in ways that give an independent measure of the source's angular momentum, which means that quantitative tests are impossible.

27.2.6 Binary Pulsar

Gravity in the solar system is very weak. Even at Mercury's orbit, the gravitational potential of the sun is only $|\Phi| \sim 3 \times 10^{-8}$. Therefore, when one expands the spacetime metric in powers of Φ, current experiments with their fractional accuracies $\sim 10^{-5}$ or worse are able to see only the first-order terms beyond Newtonian theory; i.e. terms of *first post-Newtonian order*. To move on to second post-Newtonian order, $\mathcal{O}(\Phi^2)$ beyond Newton, will require major advances in technology, or observations of astronomical systems in which Φ is far larger than 3×10^{-8}.

[1] There has been considerable controversy over the accuracy of the LAGEOS measurements; see Iorio, Ruggiero and Corda (2013) and references therein. The critics will grant an accuracy of 40%, and the proponents argue for 10%, as of December 2013.

Radio observations of binary pulsars (this subsection) provide one opportunity for such observations; gravitational-wave observations of neutron-star and black-hole binaries provide another (Secs. 27.5.4, 27.5.5, and 27.6).

The best binary pulsar for tests of general relativity is PSR1913+16, discovered by Russell Hulse and Joseph Taylor in 1974 (though others, particularly the double pulsar PSR J0737-3039, may surpass it in the future). PSR1913+16 consists of two neutron stars in a mutual elliptical orbit with period $P \sim 8$ hr and eccentricity $e \sim 0.6$. One of the stars emits pulses at a regular rate. These are received at earth with time delays due to crossing the binary orbit and other relativistic effects. We do not know *a priori* the orbital inclination or the neutron-star masses. However, we obtain one relation between these three quantities by analyzing the Newtonian orbit. A second relation comes from measuring the consequences of the combined second order Doppler shift and gravitational redshift as the pulsar moves in and out of its companion's gravitational field. A third relation comes from measuring the relativistic precession of the orbit's periastron (analog of the perihelion shift of Mercury). (The precession rate is far larger than for Mercury: about 4° per year!) From these three relations one can solve for the stars' masses and the orbital inclination, and as a check can verify that the Shapiro time delay comes out correctly. One can then use the system's parameters to predict the rate of orbital inspiral due to gravitational-radiation reaction—a phenomenon with magnitude $\sim |\Phi|^{2.5}$ beyond Newton, i.e. 2.5 post-Newtonian order (Sec. 27.5.2 below). The prediction agrees with the measurements to accuracy ~ 0.2 per cent (Weissberg, Nice and Taylor 2011) —a major triumph for general relativity!

For reviews of other tests of general relativity using binary pulsars, see Stairs (2010) and papers cited therein.

27.3 Gravitational Waves Propagating through Flat Spacetime

Gravitational waves are *ripples in the curvature of spacetime* that are emitted by violent astrophysical events, and that propagate with the speed of light. It was clear to Einstein and others, even before general relativity was fully formulated, that his theory would have to predict gravitational waves, and within months after completing the theory, Einstein (1916, 1918) worked out the those waves' basic properties.

It turns out that, after they have been emitted, gravitational waves propagate through matter with near impunity, i.e., they propagate as though in vacuum, even when other matter and fields are present. (For a proof and discussion see, e.g., Sec. 2.4.3 of Thorne, 1983). This justifies simplifying our analysis to vacuum propagation.

27.3.1 Weak, Plane Waves in Linearized Theory

Once the waves are far from their source, the radii of curvature of their phase fronts are huge compared to a wavelength, as is the radius of curvature of the spacetime through which they propagate. This means that, to high accuracy, we can idealize the waves as plane-fronted

and as propagating through flat spacetime. The appropriate formalism for describing this is the *Linearized Theory* developed in Sec. 25.9.2:

We introduce coordinates that are as nearly Lorentz as possible, so the spacetime metric can be written as

$$\boxed{g_{\alpha\beta} = \eta_{\alpha\beta} + h_{\alpha\beta} \ , \quad \text{with} \ \ |h_{\alpha\beta}| \ll 1} \tag{27.17a}$$

[Eq. (25.82)], and we call $h_{\alpha\beta}$ the waves' *metric perturbation*. We perform an "infinitesimal coordinate transformation" (gauge change)

$$x^\alpha_{\rm new}(\mathcal{P}) = x^\alpha_{\rm old}(\mathcal{P}) + \xi^\alpha(\mathcal{P}) \ , \quad \text{which produces} \quad h^{\rm new}_{\mu\nu} = h^{\rm old}_{\mu\nu} - \xi_{\mu,\nu} - \xi_{\nu,\mu} \tag{27.17b}$$

[Eqs. (25.87) and (25.88)], with the gauge-change generators $\xi^\alpha(\mathcal{P})$ chosen so as to impose the Lorenz gauge condition

$$\boxed{\bar{h}_{\mu\nu}{}^{,\nu} = 0} \tag{27.17c}$$

[Eq. (25.89)] on the new *trace-reversed metric perturbation*

$$\boxed{\bar{h}_{\mu\nu} \equiv h_{\mu\nu} - \frac{1}{2} h\, \eta_{\mu\nu} \ , \quad h \equiv \eta^{\alpha\beta} h_{\alpha\beta}} \tag{27.17d}$$

[Eqs. (25.85) and (25.84)]. In this Lorenz gauge, the vacuum Einstein field equation becomes the flat-space wave equation for $\bar{h}^{\mu\nu}$ and so also for $h^{\mu\nu}$

$$\boxed{\bar{h}_{\mu\nu,\alpha}{}^{\alpha} = h_{\mu\nu,\alpha}{}^{\alpha} = 0} \ . \tag{27.17e}$$

[Eq. (25.90)].

This is as far as we went in vacuum (far from the waves' source) in Chap. 25. We now go further: We simplify the mathematics by orienting the axes of our nearly Lorentz coordinates so the waves are planar and propagate in the z direction. Then the obvious solution to the wave equation (27.17e), and the consequence of the Lorenz gauge condition (27.17c) are

$$\bar{h}_{\mu\nu} = \bar{h}_{\mu\nu}(t-z) \ , \quad \bar{h}_{\mu 0} = -\bar{h}_{\mu z} \ . \tag{27.18}$$

There are now six independent components of the trace-reversed metric perturbation, the six spatial $\bar{h}_{ij}$; the second of Eqs. (27.18) fixes the time-space and time-time components in terms of them.

Remarkably, these six independent components can be reduced to two by a further specialization of gauge. The original infinitesimal coordinate transformation (27.17b), which brought us into Lorenz gauge, relied on four functions $\xi_\mu(\mathcal{P}) = \xi_\mu(x^\alpha)$ of four spacetime coordinates. A more restricted set of gauge-change generators, $\xi_\mu(t-z)$, that are functions solely of retarded time (and thus satisfy the wave equation) will keep us in Lorenz gauge, and can be used to annul the four components $\bar{h}_{xz}$, $\bar{h}_{yz}$, $\bar{h}_{zz}$, and $\bar{h} \equiv \eta^{\mu\nu}\bar{h}_{\mu\nu}$, whence (thanks to the Lorenz conditions $\bar{h}_{\mu 0} = -\bar{h}_{\mu z}$) all the $\bar{h}_{\mu 0}$ are also annulled. See Ex. 27.5. As a result, *the trace-reversed metric perturbation $\bar{h}_{\mu\nu}$ and the metric perturbation $h_{\mu\nu}$ are now equal, and their only nonzero components are $h_{xx} = -h_{yy}$ and $h_{xy} = +h_{yx}$.*

This very special new gauge has the name *transverse-traceless gauge* or *TT gauge* because in it the metric perturbation is purely spatial, it is transverse to the waves' propagation

direction (the z direction), and it is traceless. *It is convenient to use the notation $h^{\rm TT}_{\mu\nu}$ for the metric perturbation (27.19) in this TT gauge, and convenient to give the names h_+ and $h_\times$ to its two independent, nonzero components (which are associated with two polarization states for the waves, "+" and "×"):*

$$\boxed{h^{\rm TT}_{xx} = -h^{\rm TT}_{yy} = h_+(t-z)\ , \quad h^{\rm TT}_{xy} = +h^{\rm TT}_{yx} = h_\times(t-z)}\ . \tag{27.19}$$

The Riemann curvature tensor in this TT gauge, as in any gauge, can be expressed as

$$\boxed{R_{\alpha\beta\gamma\delta} = \frac{1}{2} h^{\rm TT}_{\{\alpha\beta,\gamma\delta\}} \equiv \frac{1}{2}(h^{\rm TT}_{\alpha\delta,\beta\gamma} + h^{\rm TT}_{\beta\gamma,\alpha\delta} - h^{\rm TT}_{\alpha\gamma,\beta\delta} - h^{\rm TT}_{\beta\delta,\alpha\gamma})} \tag{27.20}$$

[Eq. (25.80)]. Here the subscript symbol {...}, analogous to [...] for antisymmetrization and (...) for symmetrization, means the combination of four terms on the right side of the ≡ sign. Of particular interest for physical measurements is the relativistic tidal field $\mathcal{E}_{ij} = R_{i0j0}$, which produces a relative acceleration of freely falling particles [geodesic deviation; Eq. (25.34)]. Since the temporal components of $h^{\rm TT}_{\mu\nu}$ vanish, in Eq. (27.20) for R_{i0j0} the only nonzero term is the third one, in which the temporal components are derivatives, whence

$$\boxed{\mathcal{E}_{ij} = R_{i0j0} = -\frac{1}{2}\ddot{h}^{\rm TT}_{ij}}\ ; \quad \text{i.e.} \quad \boxed{\mathcal{E}_{xx} = -\mathcal{E}_{yy} = -\frac{1}{2}\ddot{h}_+(t-z)\ , \quad \mathcal{E}_{xy} = +\mathcal{E}_{yx} = -\frac{1}{2}\ddot{h}_\times(t-z)}\ . \tag{27.21}$$

Here the dots mean time derivatives: $\ddot{h}_+(t-x) \equiv \partial^2 h_+/\partial t^2$. A useful index-free way to write these equations is

$$\boxed{\boldsymbol{\mathcal{E}} = -\frac{1}{2}\ddot{\boldsymbol{h}}^{\rm TT} = -\frac{1}{2}\ddot{h}_+ \boldsymbol{e}^+ - \frac{1}{2}\ddot{h}_\times \boldsymbol{e}^\times}\ , \tag{27.22a}$$

where

$$\boxed{\boldsymbol{e}^+ = \vec{e}_x \otimes \vec{e}_x - \vec{e}_y \otimes \vec{e}_y}\ , \quad \boxed{\boldsymbol{e}^\times = \vec{e}_x \otimes \vec{e}_x + \vec{e}_y \otimes \vec{e}_y} \tag{27.22b}$$

are the *polarization tensors* associated with the + and × polarizations.

It is a very important fact that the Riemann curvature tensor is gauge-invariant. An infinitesimal coordinate transformation $x^\alpha_{\rm new}(\mathcal{P}) = x^\alpha_{\rm old}(\mathcal{P}) + \xi^\alpha(\mathcal{P})$ changes it by tiny fractional amounts of order ξ^α, by contrast with the metric perturbation, which gets changed by amounts of order itself, $\delta h_{\mu\nu} = -2\xi_{(\mu,\nu)}$, i.e. by fractional amounts of order unity (Ex. 25.19). This has two important consequences: (i) The gauge-invariant Riemann tensor (or its space-time-space-time part, the tidal tensor) is an optimal tool for discussing physical measurements (next subsection) — a much better tool, e.g., than the gauge-dependent metric perturbation. (ii) The gauge invariance of Riemann motivates us to change our viewpoint on $h^{\rm TT}_{ij}$ in the following way:

We define a dimensionless "gravitational-wave field" $h^{\rm TT}_{ij}$ to be minus twice the double time integral of the wave's tidal field

$$\boxed{h^{\rm TT}_{ij} \equiv -2\int dt \int dt\, \mathcal{E}_{ij}}\ . \tag{27.23}$$

And we regard the computation that led to Eq. (27.21) as a demonstration that it is possible to find a gauge in which the metric perturbation is purely spatial and its spatial part is equal to this gravitational-wave field, $h_{0\mu} = 0$ and $h_{ij} = h^{\rm TT}_{ij}$.

In Box 27.2, we show that, if we have found a gauge in which the metric pertubation propagates as a plane wave at the speed of light, then we can compute the gravitational-wave field $h^{\rm TT}_{ij}$ from that gauge's $h_{\alpha\beta}$ or $\bar{h}_{\alpha\beta}$ by a simple projection process. This result is useful in the theory of gravitational-wave generation; see, e.g., Sec. 27.5.2.

Box 27.2
Projecting Out the Gravitational-Wave Field $h^{\rm TT}_{ij}$

Suppose that, for some gravitational wave, we have found a gauge (not necessarily TT) in which $h_{\mu\nu} = h_{\mu\nu}(t-z)$. Then a simple calculation with Eq. (25.80) reveals that the only nonzero components of this wave's tidal field are $\mathcal{E}_{ab} = -\frac{1}{2}\ddot{h}_{ab}$, where a and b run over x and y. But by definition, $\mathcal{E}_{ab} = -\frac{1}{2}\ddot{h}^{\rm TT}_{ab}$. Therefore, in this gauge we can compute the gravitational wave field by simply throwing away all parts of $h_{\mu\nu}$ except the spatial, transverse parts: $h^{\rm TT}_{xx} = h_{xx}$, $h^{\rm TT}_{xy} = h_{xy}$, $h^{\rm TT}_{yy} = h_{yy}$.

When computing the generation of gravitational waves, it is often easier to evaluate the trace-reversed metric perturbation $\bar{h}_{\alpha\beta}$ than the metric perturbation itself [e.g., Eq. (25.91)]. But $\bar{h}_{\alpha\beta}$ differs from $h_{\alpha\beta}$ by only a trace, and the gravitational-wave field $h^{\rm TT}_{jk}$ is trace-free. *Therefore, in any gauge where $\bar{h}_{\mu\nu} = \bar{h}_{\mu\nu}(t-z)$, we can compute the gravitational-wave field $h^{\rm TT}_{jk}$ from $\bar{h}_{\mu\nu}$ by throwing away everything except its spatial, transverse part, and by then removing its trace — i.e., by projecting out the spatial, transverse, traceless part:*

$$\boxed{h^{\rm TT}_{jk} = \left(\bar{h}_{jk}\right)^{\rm TT} \ ; \text{ i.e. } h_+ = h^{\rm TT}_{xx} = \bar{h}_{xx} - \frac{1}{2}(\bar{h}_{xx}+\bar{h}_{yy}) = \frac{1}{2}(h_{xx}-h_{yy}) \ , \quad h_\times = h^{\rm TT}_{xy} = \bar{h}_{xy}} \ . \tag{1}$$

Here the symbol $\left(\bar{h}_{jk}\right)^{\rm TT}$ means "project out the spatial, transverse, traceless part".

If we rotate the spatial axes so the waves propagate along the unit spatial vector $\mathbf{n}$ instead of along $\mathbf{e}_z$, then the "speed-of-light-propagation" forms of the metric perturbation and its trace reversal become $h_{\alpha\beta} = h_{\alpha\beta}(t - \mathbf{n}\cdot\mathbf{x})$ and $\bar{h}_{\alpha\beta} = \bar{h}_{\alpha\beta}(t-\mathbf{n}\cdot\mathbf{x})$, and the TT projection can be achieved with the aid of the transverse projection tensor

$$\boxed{P^{jk} \equiv \delta^{jk} - n^j\, n^k} \ . \tag{2}$$

Specifically,

$$\boxed{h^{\rm TT}_{jk} = (\bar{h}_{jk})^{\rm TT} = P_j{}^l P_k{}^m \bar{h}_{lm} - \frac{1}{2} P_{jk} P^{lm} \bar{h}_{lm}} \ . \tag{3}$$

Here the notation is that of Cartesian coordinates with $P_j{}^k = P^{jk} = P_{jk}$.

****

EXERCISES

Exercise 27.5 *Derivation: Bringing $h_{\mu\nu}$ into TT gauge*

Consider a weak, planar gravitational wave propagating in the z direction, written in a general Lorenz gauge, Eqs. (27.18). Show that by appropriate choices of new gauge-change generators that have the plane-wave form $\xi_\mu(t-z)$, one can (i) keep the metric perturbation in Lorenz gauge, (ii) annul $\bar{h}_{xz}$, $\bar{h}_{yz}$, $\bar{h}_{zz}$, and $\bar{h} \equiv \eta^{\mu\nu}\bar{h}_{\mu\nu}$, and (iii) thereby make the only nonzero components of the metric perturbation be $h_{xx} = -h_{yy}$ and $h_{xy} = +h_{yx}$. [Hint: Show that a gauge change (27.17b) produces $\bar{h}^{\rm new}_{\mu\nu} = \bar{h}^{\rm old}_{\mu\nu} - \xi_{\mu,\nu} - \xi_{\nu,\mu} + \eta_{\mu\nu}\xi_\alpha{}^{,\alpha}$, and use this in your computations.]

****

27.3.2 Measuring a Gravitational Wave by its Tidal Forces

We seek physical insight into gravitational waves by studying the following idealized problem:

Consider a cloud of test particles that floats freely in space and is static and spherical before the waves pass. Study the wave-induced deformations of the cloud as viewed in the nearest thing there is to a rigid, orthonormal coordinate system: the local Lorentz frame (in the physical spacetime) of a "fiducial particle" that sits at the cloud's center. In that frame the displacement vector ζ^j between the fiducial particle and some other particle has components $\zeta^j = x^j + \delta x^j$, where x^j is the other particle's spatial coordinate before the waves pass, and δx^j is its coordinate displacement, as produced by the waves. By inserting this into the local-Lorentz-frame variant of the equation of geodesic deviation, Eq. (25.34), and neglecting the tiny δx^k compared to x^k on the right side, we obtain

$$\frac{d^2\delta x^j}{dt^2} = -R_{j0k0}x^k = -\mathcal{E}_{jk}x^k = \frac{1}{2}\ddot{h}^{\rm TT}_{jk}x^k \ , \tag{27.24}$$

which can be integrated twice to give

$$\boxed{\delta x^j = \frac{1}{2}h^{\rm TT}_{jk}x^k} \ . \tag{27.25}$$

Expression (27.24) is the *gravitational-wave tidal acceleration* that moves the particles back and forth relative to each other. It is completely analogous to the Newtonian tidal acceleration $-\mathcal{E}_{jk}x^k = -(\partial^2\Phi/\partial x^j\partial x^k)x^k$ by which the moon raises tides on the earth's oceans (Sec. 25.5.1).

Specialize, now, to a wave with + polarization (for which $h_\times = 0$). By inserting expression (27.19) into (27.25), we obtain

$$\delta x = \frac{1}{2}h_+ x \ , \quad \delta y = -\frac{1}{2}h_+ y \ , \quad \delta z = 0 \ . \tag{27.26}$$

This displacement is shown in Fig. 27.1a,b. Notice that, as the gravitational-wave field h_+ oscillates at the cloud's location, the cloud is left undisturbed in the z-direction (propagation direction), and in transverse planes it gets deformed into an ellipse elongated first along the x-axis (when $h_+ > 0$), then along the y-axis (when $h_+ < 0$). Because $\mathcal{E}_{xx} = -\mathcal{E}_{yy}$, i.e.,

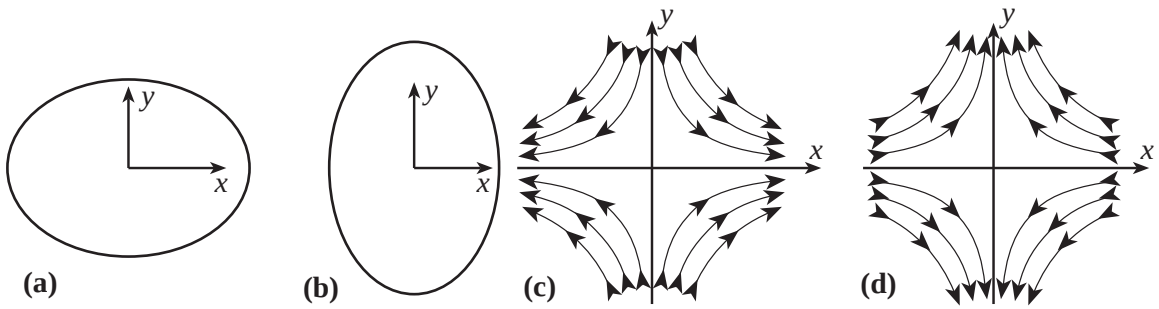

Fig. 27.1: Physical manifestations, in a particle's local Lorentz frame, of h_+ gravitational waves. (a) Transverse deformation of an initially spherical cloud of test particles at a phase of the wave when $h_+ > 0$. (b) Deformation of the cloud when $h_+ < 0$. (c) Field lines representing the acceleration field $\delta\ddot{\mathbf{x}}$ that produces the cloud's deformation, at a phase when $\ddot{h}_+ > 0$. (d) Acceleration field lines when $\ddot{h}_+ < 0$.

because $\mathcal{E}_{jk}$ is traceless, the ellipse is squashed along one axis by the same amount as it is stretched along the other, i.e., the area of the ellipse is preserved during the oscillations.

The effects of the h_+ polarization state can also be described in terms of the *tidal acceleration field* that it produces in the central particle's local Lorentz frame:

$$\frac{d^2}{dt^2}\delta\mathbf{x} = -\boldsymbol{\mathcal{E}}_+ \cdot \mathbf{x} = \frac{1}{2}\ddot{h}_+(x\mathbf{e}_x - y\mathbf{e}_y) \;, \tag{27.27}$$

where $\ddot{h}_+ \equiv \partial^2 h_+/\partial t^2$. Notice that this acceleration vector field $\delta\ddot{\mathbf{x}}$ is divergence free. Because it is divergence-free, it can be represented by lines of force, analogous to electric field lines, which point along the field and have a density of lines proportional to the magnitude of the field; and when this is done, the field lines will never end. Figure 27.1c,d shows this acceleration field at the phases of oscillation when $\ddot{h}_+$ is positive and when it is negative. Notice that the field is quadrupolar in shape, with a field strength (density of lines) that increases linearly with distance from the origin of the local Lorentz frame. The elliptical deformations of the spherical cloud of test particles shown in Fig. 27.1a,b are the responses of that cloud to this quadrupolar acceleration field. The polarization state which produces these accelerations and deformations is called the + state because of the orientation of the axes of the quadrupolar acceleration field (Fig. 27.1c,d).

Turn, next, to the × polarization state. In this state the deformations of the initially circular ring are described by

$$\delta x = \frac{1}{2}h_\times y \;, \quad \delta y = \frac{1}{2}h_\times x \;, \quad \delta z = 0 \;. \tag{27.28}$$

These deformations, like those for the + state, are purely transverse; they are depicted in Fig. 27.2a,b. The acceleration field that produces these deformations is

$$\frac{d^2}{dt^2}\delta\mathbf{x} = -\boldsymbol{\mathcal{E}}_\times \cdot \mathbf{x} = \frac{1}{2}\ddot{h}_\times(y\mathbf{e}_x + x\mathbf{e}_y) \;. \tag{27.29}$$

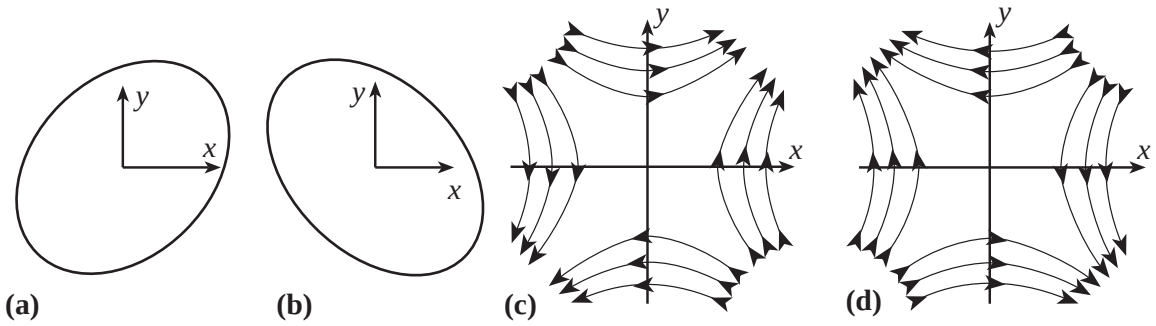

Fig. 27.2: Physical manifestations, in a particle's local Lorentz frame, of $h_\times$ gravitational waves. (a) Deformation of an initially circular sphere of test particles at a phase of the wave when $h_\times > 0$. (b) Deformation of the sphere when $h_\times < 0$. (c) Field lines representing the acceleration field $\delta\ddot{\mathbf{x}}$ that produces the sphere's deformation, at a phase of the wave when $\ddot{h}_\times > 0$. (d) Acceleration field lines when $\ddot{h}_\times < 0$.

This acceleration field, like the one for the + polarization state, is divergence free and quadrupolar; the field lines describing it are depicted in Fig. 27.2c,d. The name "× polarization state" comes from the orientation of the axes of this quadrupolar acceleration field.

Planar gravitational waves can also be depicted in terms of the tendex and vortex lines associated with their tidal tensor field $\boldsymbol{\mathcal{E}}$ and frame-drag tensor field $\boldsymbol{\mathcal{B}}$; see Box 27.3.

In defining the gravitational-wave fields h_+ and $h_\times$, we have relied on a choice of (local Lorentz) reference frame, i.e. a choice of local Lorentz basis vectors $\vec{e}_\alpha$. Exercise 27.6 explores how these fields change when the basis is changed. The conclusions are simple: (i) When one rotates the transverse basis vectors $\vec{e}_x$ and $\vec{e}_y$ through an angle ψ, then h_+ and $h_\times$ rotate through 2ψ in the sense that:

$$\boxed{(h_+ + ih_\times)_{\rm new} = (h_+ + ih_\times)_{\rm old} e^{2i\psi} \ , \quad \text{when} \quad (\vec{e}_x + i\vec{e}_y)_{\rm new} = (\vec{e}_x + i\vec{e}_y)e^{i\psi}} \ . \qquad (27.30)$$

(ii) When one boosts from an old frame to a new one moving at some other speed, but chooses the old and new spatial bases such that (a) the waves propagate in the z direction in both frames and (b) the plane spanned by $\vec{e}_x$ and $\vec{\kappa} \equiv \vec{e}_0 + \vec{e}_z$ =(propagation direction in spacetime) is the same in both frames, then h_+ and $h_\times$ are the same in the two frames—i.e., they are scalars under such a boost!

****

EXERCISES

Exercise 27.6 *Derivation: Behavior of h_+ and $h_\times$ under rotations and boosts*

(a) Derive the behavior (27.30) of h_+ and $h_\times$ under rotations in the transverse plane. [Hint: Write the gravitational-wave field, viewed as a geometric object, as $\boldsymbol{h}^{\rm TT} = \Re\left[(h_+ + ih_\times)(\boldsymbol{e}^+ - i\boldsymbol{e}^\times)\right]$, where $\boldsymbol{e}^+ = (\vec{e}_x \otimes \vec{e}_x - \vec{e}_y \otimes \vec{e}_y)$ and $\boldsymbol{e}^\times = (\vec{e}_x \otimes \vec{e}_y + \vec{e}_y \otimes \vec{e}_x)$ are the polarization tensors associated with + and × polarized waves [Eqs. (27.22b)]. Then show that $\mathbf{e}_+ - i\mathbf{e}_\times$ rotates through -2ψ, and use this to infer the desired result.]

Box 27.3

T2 Tendex and Vortex Lines for a Gravitational Wave

A plane gravitational wave with + polarization, propagating in the z direction, has as its only nonzero tidal-field components $\mathcal{E}_{xx} = -\mathcal{E}_{yy} = -\frac{1}{2}\ddot{h}_+(t-z)$ [Eq. (27.21)]. This tidal field's eigenvectors are $\mathbf{e}_x$ and $\mathbf{e}_y$, so its tendex lines (Boxes 25.2 and 26.3) are straight lines pointing along these basis vectors, i.e., the solid lines in this picture:

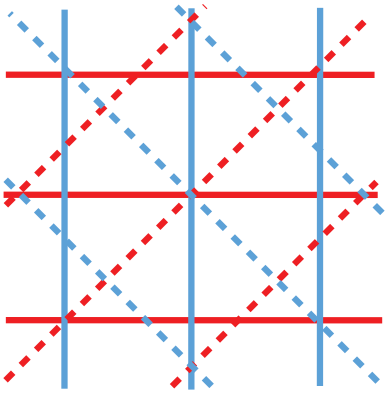

These lines' tendicities $\mathcal{E}_{xx}$ and $\mathcal{E}_{yy}$ are equal and opposite, so one set of lines stretches (is red) and the other squeezes (is blue). As the wave propagates, each line's tendicity oscillates, so its color oscillates between red and blue.

From the Maxwell-like Bianchi identity $\partial\boldsymbol{\mathcal{B}}/\partial t = -(\boldsymbol{\nabla}\times\boldsymbol{\mathcal{E}})^{\rm S}$ (Box 25.2), with $\boldsymbol{\mathcal{E}}$ a function of $t-\mathbf{n}\cdot\mathbf{x}$ and $\mathbf{n}=\mathbf{e}_z$ the wave's propagation direction, we infer that the wave's frame-drag field and tidal field are related by $\boldsymbol{\mathcal{B}} = (\mathbf{n}\times\boldsymbol{\mathcal{E}})^{\rm S}$. This means that the nonzero components of $\boldsymbol{\mathcal{B}}$ are $\mathcal{B}_{xy}=\mathcal{B}_{yx}=\mathcal{E}_{xx}=-\mathcal{E}_{yy}=-\frac{1}{2}\ddot{h}_+(t-z)$. Therefore, the gravitational wave's vortex lines are the dashed lines in the figure above (where the propagation direction, $\mathbf{n}=\mathbf{e}_z$ is out of the screen or paper, toward you).

Electric and magnetic field lines are generally drawn with line densities proportional to the magnitude of the field — a convention motivated by flux conservation. Not so for tendex and vortex lines, which have no corresponding conservation law. Instead, their field strengths (tendicities and vorticities) are usually indicated by color coding; see, e.g., Nichols et. al. (2012).

Most discussions of gravitational waves (including the text of this chapter) focus on their tidal field $\boldsymbol{\mathcal{E}}$ and its physical stretch and squeeze, and ignore the frame-drag field with its differential precession (twisting) of gyroscopes. The reason is that modern technology is able to detect and monitor the stretch and squeeze, but the precession is far too small to be detected.

(b) Show that, with the orientations of spatial basis vectors described after Eq. (27.30), h_+ and $h_\times$ are unchanged by boosts.

****

27.3.3 Gravitons and their Spin and Rest Mass

Most of the above features of gravitational waves (though not expressed in this language) were clear to Einstein in 1918. Two decades later, as part of the effort to understand quantum fields, Markus Fierz and Wolfgang Pauli (1939), at the Eidgenössische Technische Hochschule (ETH) in Zurich, Switzerland, formulated a classical theory of linear fields of arbitrary spin so designed that the fields would be quantizable by canonical methods. Remarkably, their canonical theory for a field of spin two and zero rest mass is identical to general relativity with nonlinear effects removed, and the plane waves of that spin-two theory are identical to the waves described above. When quantized by canonical techniques, these waves are carried by zero-rest-mass, spin-two gravitons.

One can see by simple arguments that the gravitons which carry gravitational waves must have zero rest mass and spin two:

First: Fundamental principles of quantum theory guarantee that any wave that propagates in vacuum with the speed of light must be carried by particles which have that same speed, i.e., particles whose 4-momenta are null, i.e., particles which have zero rest mass. General relativity predicts that gravitational waves propagate with the speed of light. Therefore, its gravitons must have zero rest mass.

Next: Consider any plane-wave field (neutrino, electromagnetic, gravitational, ...) that propagate at the speed of light in the z-direction of a (local) Lorentz frame. At any moment of time examine any physical manifestation of that field, e.g., the acceleration field it produces on test particles. Rotate that manifestation of the field around the z axis, and ask what is the minimum angle of rotation required to bring the field back to its original configuration. Call that minimum angle, $\theta_{\rm ret}$, the waves' *return angle*. The spin S of the particles that carry the wave will necessarily be related to that return angle by[2]

$$\boxed{S = \frac{360 \text{ degrees}}{\theta_{\rm ret}}} \,. \tag{27.31}$$

This simple formula corresponds to the elegant mathematical statement that "the waves generate an irreducible representation of order $S = 360\,\text{degrees}/\theta_{\rm ret}$ of that subgroup of the Lorentz group which leaves their propagation vector unchanged (the 'Little group' of the rotation vector)." For electromagnetic waves, a physical manifestation is the electric field, which is described by a vector lying in the x–y plane; if one rotates that vector about the z-axis (propagation axis), it returns to its original orientation after a return angle $\theta_{\rm ret} = 360$ degrees. Correspondingly, the spin of the particle which carries the electromagnetic wave (the photon) is one. For neutrinos, the return angle is $\theta_{\rm ret} = 720$ degrees; and correspondingly the spin of a neutrino is $\frac{1}{2}$. For gravitational waves, the physical manifestations include the deformation of a sphere of test particles (Figs. 27.1a,b and 27.2a,b) and the acceleration fields (Figs. 27.1c,d and 27.2c,d). Both the deformed, ellipsoidal spheres and the quadrupolar lines of force return to their original orientations after rotation through $\theta_{\rm ret} = 180$ degrees; and correspondingly, the graviton must have spin two. This spin 2 also shows up in the rotation factor $e^{i2\psi}$ of Eq. (27.30).

[2]For spin 0 this formula fails. Spin 0 corresponds to circular symmetry around the spin axis.

Although Fierz and Pauli (1939) showed us how to quantize linearized general relativity, the quantization of full, nonlinear general relativity remains a difficult subject of current research, to which we shall return briefly in the next chapter.

27.4 Gravitational Waves Propagating through Curved Spacetime

Richard Isaacson (1968a,b) has developed a geometric-optics formulation of the theory of gravitational waves propagating through curved spacetime, and as a byproduct he has given a rigorous mathematical description of the waves' stress-energy tensor and thence the energy and momentum carried by the waves. In this section we shall sketch the main ideas and results of Isaacson's analysis.

The foundation for the analysis is a 2-lengthscale expansion $\lambda\!\!\!^{-}/\mathcal{L}$ like we used in Sec. 7.3 when formulating geometric optics: For any physical quantity, we identify the wave contribution as the portion that varies on some short lengthscale $\lambda\!\!\!^{-} = \lambda/2\pi$ (the waves' reduced wavelength), and the background as the portion that varies on a far longer lengthscale $\mathcal{L}$ (which is less than or of order the background's spacetime radius of curvature $\mathcal{R}$); see Fig. 27.3.

To make this idea work, analytically, we must use "steady" coordinates, i.e., coordinates that are smooth, to as great an extent as the waves permit, on lengthscales shorter than $\mathcal{L}$. In such coordinates, components of the spacetime metric $g_{\alpha\beta}$ and of the Riemann curvature tensor $R_{\alpha\beta\gamma\delta}$ split into background plus waves,

$$g_{\alpha\beta} = g^{\rm B}_{\alpha\beta} + h_{\alpha\beta} \ , \quad R_{\alpha\beta\gamma\delta} = R^{\rm B}_{\alpha\beta\gamma\delta} + R^{\rm GW}_{\alpha\beta\gamma\delta} \ , \tag{27.32a}$$

where the background quantitities are defined as the averages (denoted $\langle ... \rangle$) of the full quantities over lengthscales long compared to $\lambda\!\!\!^{-}$ and short compared to $\mathcal{L}$:

$$g^{\rm B}_{\alpha\beta} \equiv \langle g_{\alpha\beta} \rangle \ , \quad R^{\rm B}_{\alpha\beta\gamma\delta} \equiv \langle R_{\alpha\beta\gamma\delta} \rangle \ . \tag{27.32b}$$

To assist us in solving the Einstein equation, we treat the Einstein tensor $G_{\alpha\beta}$ a bit differently from the metric and Riemann. We begin by expanding $G_{\alpha\beta}$ as a power series in the metric perturbation $h_{\alpha\beta}$: $G_{\alpha\beta} = G^{\rm B}_{\alpha\beta} + G^{(1)}_{\alpha\beta} + G^{(2)}_{\alpha\beta} + ...$ Here $G^{\rm B}_{\alpha\beta}$ is the Einstein tensor

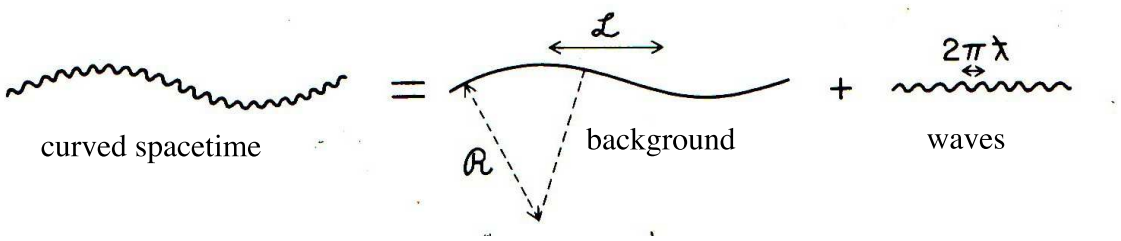

Fig. 27.3: Heuristic embedding diagram for the decomposition of curved spacetime into a background spacetime plus gravitational waves

computed from the background metric $g^{\rm B}_{\alpha\beta}$, $G^{(1)}_{\alpha\beta}$ is linear in $h_{\alpha\beta}$, $G^{(2)}_{\alpha\beta}$ is quadratic, etc. We then split $G_{\alpha\beta}$ into its rapidly varying part, which is simply $G^{(1)}_{\alpha\beta}$ at leading order, and its smoothly varying part, which through quadratic order is $\langle G_{\alpha\beta}\rangle = G^{\rm B}_{\alpha\beta} + \langle G^{(2)}_{\alpha\beta}\rangle$. The vacuum Einstein equation $G_{\alpha\beta} = 0$ will be satisfied only if the rapidly and smoothly varying parts both vanish.

In Sec. 27.4.1, by setting the fast-varying part $G^{(1)}_{\alpha\beta}$ to zero, we shall obtain a wave equation, in the background curved spacetime, for $h_{\alpha\beta}$ (the gravitational waves), which we can solve (Sec. 27.4.2) using the geometric optics approximation that underlies this analysis. Then, in Sec. 27.4.3, by setting the slowly varying part $G^{B}_{\alpha\beta} + \langle G^{(2)}_{\alpha\beta}\rangle$ to zero, we shall obtain Isaacson's description of gravitational-wave energy and momentum.

27.4.1 Gravitational Wave Equation in Curved Spacetime

The metric perturbation $h_{\alpha\beta}$ can be regarded as a tensor field that lives in the background spacetime.[3] The rapidly varying part of the Einstein equation, $G^{(1)}_{\alpha\beta} = 0$, gives rise to a wave equation for this tensorial metric perturbation (Isaacson 1968a; Secs. 35.13 and 35.14 of MTW). We can infer this wave equation most easily from a knowledge of the form it takes in any local Lorentz frame of the background (with size $\gg \lambda$ but $\ll \mathcal{L}$). In such a frame, $G^{(1)}_{\alpha\beta} = 0$ must reduce to the field equation of linearized theory [the vacuum version of Eq. (25.83)]. And if we introduce Lorenz gauge [Eq. (27.17c)], then $G^{(1)}_{\alpha\beta} = 0$ must become, in a local Lorentz frame, the vacuum wave equation (27.17e). The frame-invariant versions of these local-Lorentz-frame equations, in the background spacetime, should be obvious:

The trace-reversed metric perturbation (27.17d) in frame-invariant form must become

$$\bar{h}_{\mu\nu} \equiv h_{\mu\nu} - \frac{1}{2} h\, g^{\rm B}_{\mu\nu} \ , \quad h \equiv g^{\alpha\beta}_{\rm B} h_{\alpha\beta} \ . \tag{27.33a}$$

The Lorenz-gauge condition (27.17c) must become

$$\bar{h}_{\mu\nu}{}^{|\nu} = 0 \ , \tag{27.33b}$$

where the | denotes a gradient in the background spacetime (i.e., a covariant derivative computed using connection coefficients constructed from $g^{\rm B}_{\mu\nu}$). And the gravitational wave equation (Einstein field equation) (27.17e) must become

$$\bar{h}_{\mu\nu|\alpha}{}^{\alpha} = 0 \tag{27.33c}$$

plus curvature coupling terms such as $R^{\rm B}_{\alpha\mu\beta\nu}\bar{h}^{\alpha\beta}$ that result from the noncommutation of the double gradients. The curvature coupling terms have magnitude $h/\mathcal{R}^2 \lesssim h/\mathcal{L}^2$ (where $\mathcal{R}$ is the radius of curvature of the background spacetime; cf. Fig. 27.3), while the terms kept in Eq. (27.33c) have the far larger magnitude h/λ^2, so the curvature coupling terms can be (and are) neglected.

[3] Actually, this requires that we restrict the coordinates to be steady.

27.4.2 Geometric-Optics Propagation of Gravitational Waves

When one solves Eqs. (27.33) *using the geometric optics techniques that we developed in Sec. 7.3,* one obtains precisely the results that one should expect, knowing the solution (27.18) for weak, planar gravitational waves in flat spacetime (linearized theory): (i) If we split $h_{\mu\nu}$ up into two polarization pieces + and ×, each with its own rapidly varying phase φ and slowly varying amplitude $\mathsf{A}_{\mu\nu}$, then the Lorenz-gauge, trace-reversed metric perturbation for each piece takes the standard geometric-optics form [Eq. (7.20)]:

$$h_{\mu\nu} = \Re(\mathsf{A}_{\mu\nu} e^{i\varphi}) \ . \tag{27.34a}$$

(ii) Corresponding to the fact that the linearized-theory waves propagate in a straight line (z direction) and travel at the speed of light, *the geometric-optics waves propagate through curved spacetime on rays that are null geodesics.* More specifically: the wave vector $\vec{k} = \vec{\nabla}\varphi$ is tangent to the null-ray geodesics, and φ is constant along a ray and hence is a rapidly varying function of the retarded time τ_r at which the source (in its own reference frame) emitted the ray:

$$\varphi = \varphi(\tau_r) \ , \quad \vec{k} = \vec{\nabla}\varphi \ , \quad \vec{k}\cdot\vec{k} = 0 \ , \quad \nabla_{\vec{k}}\,\vec{k} = 0 \ , \quad \nabla_{\vec{k}}\varphi = 0 \ . \tag{27.34b}$$

(iii) Corresponding to the fact that the x and y axes that define the two polarizations in linearized theory remain fixed as the wave propagates, for each polarization we can split the amplitude $\mathsf{A}_{\mu\nu}$ up into a scalar amplitude A_+ or $\mathsf{A}_\times$, and a polarization tensor $\boldsymbol{e}^+$ or $\boldsymbol{e}^\times$ (like those of Ex. 27.6), and *the polarization tensors get parallel transported along the rays*:

$$\mathsf{A}_{\mu\nu} = \mathsf{A}\, e_{\mu\nu} \ , \quad \nabla_{\vec{k}}\,\boldsymbol{e} = 0 \ . \tag{27.34c}$$

(iv) Because gravitons are conserved (cf. the conservation of quanta in our very general treatment of geometric optics, Sec. 7.3.2), the flux of gravitons (which is proportional to the square A^2 of the scalar amplitude; Sec. 27.4.3 below), times the cross sectional area $\mathcal{A}$ of a bundle of rays that are carrying the gravitons, must be constant; therefore, *the scalar wave amplitude* A *must die out as 1/(square root of cross sectional area* $\mathcal{A}$ *of a bundle of rays):*

$$\mathsf{A} \propto 1/\sqrt{\mathcal{A}} \ . \tag{27.34d}$$

Now, just as the volume of a 3-dimensional fluid element, for a perfect fluid, changes at the rate $dV/d\tau = \vec{\nabla}\cdot\vec{u}$, where $\vec{u}$ is the 4-velocity of the fluid [Eq. (2.65)], so (it turns out), the cross sectional area of a bundle of rays increases as $\nabla_{\vec{k}}\,\mathcal{A} = \vec{\nabla}\cdot\vec{k}$. Therefore, the transport law for the wave amplitude, $\mathsf{A} \propto 1/\sqrt{\mathcal{A}}$, becomes

$$\nabla_{\vec{k}}\mathsf{A} = -\frac{1}{2}(\vec{\nabla}\cdot\vec{k})\mathsf{A} \ . \tag{27.34e}$$

Equations (27.34) are derived more rigorously by Isaacson (1968a) and in Sec. 35.14 of MTW. They can be used to compute the influence of the cosmological curvature of our universe, and the gravitational fields of intervening bodies, on the propagation of graviational

waves from their sources to the earth. Once the waves have reached earth, we can compute the measured gravitational wave fields h_+ and $h_\times$ by projecting out the spatial transverse-traceless parts of $h_{\mu\nu} = \Re(\mathsf{A} e_{\mu\nu}\, e^{i\varphi})$, as discussed in Box 27.2.

The geometric-optics propagation of gravitational waves, as embodied in Eqs. (27.34), is essentially identical to that of electromagnetic waves: Both waves, gravitational and electromagnetic, propagate along rays that are null geodesics. Both parallel transport their polarizations. Both are carried by quanta that are conserved as they propagate along bundles of rays and as a result both have scalar amplitudes that vary as $\mathsf{A} \propto 1/\sqrt{\mathcal{A}}$*, where* $\mathcal{A}$ *is the cross sectional area of a ray bundle.*

Therefore, gravitational waves must exhibit exactly the same vacuum propagation phenomena as electromagnetic waves: Doppler shifts, cosmological redshifts, gravitational redshifts, gravitational deflection of rays, and gravitational lensing!

In Ex. 27.14 below, we shall illustrate this geometric optics propagation of gravitational waves by applying it to the waves from a binary system, which travel outward through our expanding universe.

Exercise 27.7 explores an application where geometric optics breaks down due to diffraction.

****

EXERCISES

Exercise 27.7 ***Example: Gravitational lensing of gravitational waves by the sun*

Gravitational waves from a distant source travel through the sun with impunity (negligible absorption and scattering) and their rays are gravitationally deflected. The sun is quite centrally condensed, so most of the deflection is produced by a central region with mass $M_c \simeq 0.3 M_\odot$ and radius $R_c \simeq 10^5\text{km} \simeq R_\odot/7$, and the maximum deflection angle is $\Delta\phi \simeq 4M_c/R_c$ [Eq. (27.7)]. A few of the deflected rays, along which the waves propagate according to geometric optics, are shown in Fig. 27.4.

(a) Show that the rays are brought to an imperfect focus and thence produce *caustics* (Sec. 7.5) at a distance from the sun (the focal length) $\mathfrak{f} \sim R_c^2/4M_c \sim 20$ AU, which is near the orbit of Uranus.

(b) If the waves were to have arbitrarily small wavelength λ, then at the caustics, their wave fields h_+ and $h_\times$ would become divergently large (Sec. 7.5). Finite wavelength

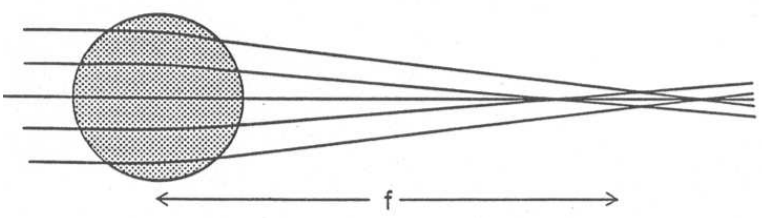

Fig. 27.4: Some gravitational-wave rays that pass through the sun are brought to an imperfect focus at a distance $\mathfrak{f}$, the focal length.

causes diffraction near the caustics (Sec. 8.6). Explain why the focused field thereby gets smeared out over a region with transverse size $\sigma \sim (\lambda/2R_c)\mathfrak{f} \sim (\lambda/8M_c)R_c$. [Hint: see Eq. 8.9 and associated discussion.]

(c) Explain why, if $\sigma \ll R_c$ (i.e. if $\lambda \ll 8M_c \sim 3M_\odot$), there is substantial focusing and the field near the caustics is strongly amplified, but if $\sigma \gtrsim R_c$ (i.e., $\lambda \gg 3M_\odot$) there is only small or no focusing. Explain why there are not likely to be any strong gravitational wave sources in the universe that emit wavelengths shorter than $3M_\odot \sim 5$ km and therefore get strongly lensed by the sun.

****

27.4.3 Energy and Momentum in Gravitational Waves

Turn, now, from the rapidly varying piece of the vacuum Einstein equations, $G^{(1)}_{\mu\nu} = 0$, to the piece that is averaged over scales long compared to λ and short compared to $\mathcal{L}$:

$$G^{\rm B}_{\alpha\beta} + \langle G^{(2)}_{\alpha\beta}\rangle = 0 \ . \tag{27.35}$$

(Recall that $G^{\rm B}_{\alpha\beta}$ is the Einstein tensor constructed from the slowly varying background metric, and $G^{(2)}_{\alpha\beta}$ is the piece of the full Einstein tensor that is quadratic in the rapidly varying metric perturbation $h_{\mu\nu}$ and that therefore does not average to zero.)

Notice that equation (27.35) can be brought into the standard form for Einstein's equation in the background spacetime,

$$\boxed{G^{\rm B}_{\alpha\beta} = 8\pi T^{\rm GW}_{\alpha\beta}} \ , \tag{27.36}$$

by moving $\langle G^{(2)}_{\alpha\beta}\rangle$ to the right hand side and then attributing to the waves a stress-energy tensor defined by

$$T^{\rm GW}_{\alpha\beta} = -\frac{1}{8\pi}\langle G^{(2)}_{\alpha\beta}\rangle \ . \tag{27.37}$$

Because this stress-energy tensor involves an average over a few wavelengths, its energy density, momentum density, energy flux, and momentum flux are *not defined* on lengthscales shorter than a wavelength. One cannot say how much energy or momentum resides in the troughs of the waves and how much in the crests. One can only say how much total energy there is in a region containing a few or more wavelengths. However, once one has reconciled oneself to this amount of nonlocality, one finds that $T^{\rm GW}_{\alpha\beta}$ has all the other properties that one expects of any good stress-energy tensor. Most especially, in the absence of coupling of the waves to matter (the situation we are treating), it obeys the standard conservation law

$$\boxed{T^{{\rm GW}\,\alpha\beta}{}_{|\beta} = 0} \ , \tag{27.38}$$

where, as above, "$|$" denotes the covariant derivative in the background spacetime, i.e. using the connection coefficients of $g^B_{\alpha\beta}$. This law is a direct consequence of the averaged field

equation (27.36) and the contracted Bianchi identity for the background spacetime $G^{\mathrm{B}\,\alpha\beta}{}_{|\beta} = 0$.

By grinding out the second-order perturbation of the Einstein tensor and inserting it into Eq. (27.37), performing several integrations by parts in the average $\langle \ldots \rangle$, and expressing the result in terms of h_+ and $h_\times$, one arrives at the following simple expression for $T^{\rm GW}_{\alpha\beta}$ in terms of the wave fields h_+ and $h_\times$:

$$\boxed{T^{\rm GW}_{\alpha\beta} = \frac{1}{16\pi}\langle h_{+,\alpha}h_{+,\beta} + h_{\times,\alpha}h_{\times,\beta}\rangle}\,. \tag{27.39}$$

[For details of the derivation, see Isaacson (1968b) or Secs. 35.13 and 35.15 of MTW.]

Let us examine this stress-energy tensor in a local Lorentz frame of the background spacetime where the waves are locally plane and are propagating in the z direction—the kind of frame we used in Sec. 27.3.2 above when exploring the properties of gravitational waves. Because, in this frame, $h_+ = h_+(t-z)$ and $h_\times = h_\times(t-z)$, the only nonzero components of Eq. (27.39) are

$$\boxed{T^{\rm GW\;00} = T^{\rm GW\;0z} = T^{\rm GW\;z0} = T^{\rm GW\;zz} = \frac{1}{16\pi}\langle \dot h_+^2 + \dot h_\times^2\rangle}\,. \tag{27.40}$$

This has the same form as the stress-energy tensor for a plane electromagnetic wave propagating in the z direction, and the same form as the stress-energy tensor for any collection of zero-rest-mass particles moving in the z-direction [cf. Eq. (3.30d)], as it must since the gravitational waves are carried by zero-rest-mass gravitons just as electromagnetic waves are carried by zero-rest-mass photons.

Suppose that the waves have frequency $\sim f$ and that the amplitudes of oscillation of h_+ and $h_\times$ are $\sim h_{\rm amp}$. Then by inserting factors of G and c into Eq. (27.40) [i.e., by switching from geometrized units to conventional units] and by setting $\langle(\partial h_+/\partial t)^2\rangle \simeq \frac{1}{2}(2\pi f h_{\rm amp})^2$ and similarly for $h_\times$, we obtain the following approximate expression for the energy flux in the waves:

$$T^{\rm GW\;0z} \simeq \frac{\pi}{4}\frac{c^3}{G}f^2h_{\rm amp}^2 \simeq 300\frac{\rm ergs}{\rm cm^2\ sec}\left(\frac{f}{1\ \rm kHz}\right)^2\left(\frac{h_{\rm amp}}{10^{-21}}\right)^2\,. \tag{27.41}$$

The numbers in this equation correspond to a strongly emitting, highly asymmetric supernova or pair of colliding neutron stars in the Virgo cluster of galaxies. Contrast this huge gravitational-wave energy flux with the peak electromagnetic flux at the height of a supernova, $\sim 10^{-9}$ erg cm^{-2} sec^{-1}; but note that the gravitational waves should last for only a few milliseconds, while the strong electromagnetic output lasts for weeks.

Corresponding to the huge energy flux (27.41) in an astrophysically interesting gravitational wave is a huge *mean occupation number* for the quantum states of the gravitational-wave field, i.e., a huge value for the number of spin-2, zero-rest-mass gravitons in each quantum state. To compute that occupation number, we shall evaluate the volume in phase space occupied by the waves from an extreme supernova and then divide by the volume occupied by each quantum state (cf. Sec. 3.2.5). At a time when the waves have reached a distance r from the source, they occupy a spherical shell of area $4\pi r^2$ and thickness of order $10\lambda\!\!\!^{-}$, where $\lambda\!\!\!^{-} = 1/(2\pi f)$ is their reduced wavelength, so their volume in physical space is

$\mathcal{V}_x \sim 100 r^2 \lambda\!\!\!^{-}$. As seen by observers whom the waves are passing, they come from a solid angle $\Delta\Omega \sim (2\lambda\!\!\!^{-}/r)^2$ centered on the source, and they have a spread of angular frequencies ranging from $\omega \sim \frac{1}{2} c/\lambda\!\!\!^{-}$ to $\omega \sim 2c/\lambda\!\!\!^{-}$. Since each graviton carries an energy $\hbar\omega = \hbar c/\lambda\!\!\!^{-}$ and a momentum $\hbar\omega/c = \hbar/\lambda\!\!\!^{-}$, the volume that they occupy in momentum space is $\mathcal{V}_p \sim (2\hbar/\lambda\!\!\!^{-})^3 \Delta\Omega$, i.e., $\mathcal{V}_p \sim 10\hbar^3/(\lambda r^2)$. The gravitons' volume in phase space, then, is

$$\mathcal{V}_x \mathcal{V}_p \sim 1000\hbar^3 \sim 4(2\pi\hbar)^3 \; . \tag{27.42}$$

Since each quantum state for a zero rest-mass particle occupies a volume $(2\pi\hbar)^3$ in phase space [Eq. (3.17) with $g_s = 1$], this means that the total number of quantum states occupied by the gravitons is of order unity! Correspondingly, the mean occupation number of each occupied state is of order the total number of gravitons emitted, which (since the total energy radiated when two neutron stars collide might be of order $10^{-2} M_\odot c^2 \sim 10^{52}$ ergs, and each graviton carries an energy $\hbar c/\lambda\!\!\!^{-} \sim 10^{-23}$ erg), is

$$\eta \sim 10^{75} \; . \tag{27.43a}$$

This is the mean occupation number from the viewpoint of the emitter.

A detector on earth has available to it only those gravitons that pass through a region with transverse size of order their wavelength λ — which means a fraction $\sim \lambda^2/(4\pi r)^2 \sim 10^{-33}$ of the emitted waves' volume. We can think of the detector as collapsing the gravitons' wave function into that volume. The number of available quantum states is still of order unity (demonstrate this!), but the number of gravitons occupying them is reduced by $\sim 10^{-33}$, so from the detector's viewpoint, the mean occupation number is

$$\eta_{\rm collapsed} \sim 10^{75} 10^{-33} \sim 10^{42} \tag{27.43b}$$

Whichever viewpoint one takes, the occupation number is enormouns. It guarantees that the waves behave exceedingly classically; quantum-mechanical corrections to the classical theory have fractional magnitude $1/\sqrt{\eta} \sim 10^{-37}$ or $\sim 10^{-21}$.

27.5 The Generation of Gravitational Waves

When analyzing the generation of gravitational waves, it is useful to divide space around the source (in the source's rest frame) into the regions shown in Fig. 27.5.

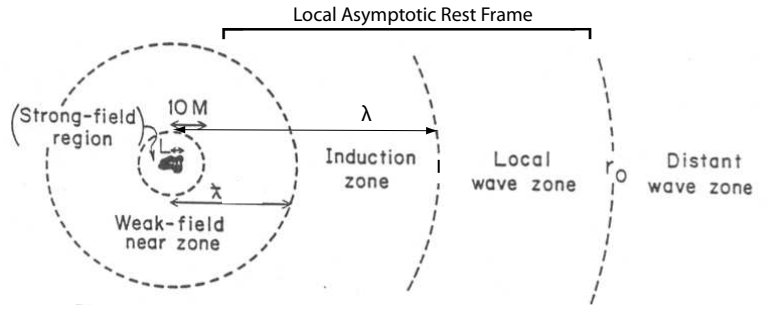

Fig. 27.5: Regions of space around a source of gravitational waves.

If the source has size $L \lesssim M$, where M is its mass, then spacetime is strongly curved inside and near it, and we refer to it as a *strong-gravity source*. The region with radii (measured from its center of mass) $r \lesssim 10M$ is called the source's *strong-field region*. Examples of strong-gravity sources are vibrating or spinning neutron stars, and merging binary black holes. The region with radii $10M \lesssim r \lesssim \lambda\!\!\!^{-} =$ (the reduced wavelength of the emitted waves) is called the source's *weak-field near zone*. In this region, the source's gravity is fairly well approximated by Newtonian theory and a Newtonian gravitational potential Φ. As in electromagnetic theory, the region $\lambda\!\!\!^{-} \lesssim r \lesssim \lambda$ is called the *induction zone* or the *transition zone*. The *wave zone* begins at $r \sim \lambda = 2\pi\lambda\!\!\!^{-}$.

It is useful to divide the wave zone into two parts: A part near the source ($r \lesssim r_o$ for some r_o) called the *local wave zone*, in which the spacetime curvature of external bodies and of the universe as a whole are unimportant, and the *distant wave zone* ($r \gtrsim r_o$), in which the emitted waves are significantly affected by external bodies and the external universe, i.e., by background spacetime curvature. The theory of gravitational-wave generation deals with computing, from the source's dynamics, the gravitational waves in the local wave zone. Propagation of the waves to earth is dealt with by using geometric optics (or other techniques) to carry the waves from the local wave zone outward, through the distant wave zone, to earth.

The entire region in which gravity is weak and the spacetme curvature of external bodies and the universe are unimportant, ($10M \lesssim r \lesssim r_o$) — when viewed in nearly Lorentz coordinates in which the source is at rest — is called the source's *local asymptotic rest frame*.

27.5.1 Multipole-moment expansion

The electromagnetic waves emitted by a dynamical charge distribution are usually expressed as a sum over the source's multipole moments. There are two families of moments: the electric moments (moments of the electric charge distribution) and the magnetic moments (moments of the electric current distribution).

Similarly, the gravitational waves emitted by a dynamical distribution of mass-energy and momentum can be expressed, in the local wave zone, as a sum over multipole moments. Again there are two families of moments: the *mass moments* (moments of the mass-energy distribution) and the *current moments* (moments of the mass-current distribution, i.e. the momentum distribution). The multipolar expansion of gravitational waves is developed in great detail in Thorne (1980) and in Blanchet (2014). In this section we shall sketch and explain its qualitative and order-of-magnitude features.

In the source's weak-gravity near zone (if it has one), the mass moments show up in the time-time part of the metric in a form familiar from Newtonian theory

$$g_{00} = -(1 + 2\Phi) = -1 \;\&\; \frac{\mathcal{I}_0}{r} \;\&\; \frac{\mathcal{I}_1}{r^2} \;\&\; \frac{\mathcal{I}_2}{r^3} \;\&\; \ldots \; . \tag{27.44}$$

[cf. Eq. (25.79)]. Here r is radius, $\mathcal{I}_\ell$ is the mass moment of order ℓ, and "&" means "plus a term with the form", i.e. a term whose magnitude and parameter dependence are shown but whose multiplicative numerical coefficients do not interest us, at least not for the moment. The mass monopole moment $\mathcal{I}_0$ is the source's mass, and the mass dipole moment $\mathcal{I}_1$ can be

made to vanish by placing the origin of coordinates at the center of mass [Eq. (25.96) and Ex. 25.21].

Similarly, in the source's weak-gravity near zone, its current moments $\mathcal{S}_\ell$ show up in the space-time part of the metric

$$g_{0j} = \frac{\mathcal{S}_1}{r^2} \,\&\, \frac{\mathcal{S}_2}{r^3} \,\&\, \ldots \,. \tag{27.45}$$

Just as there is no magnetic monopole moment in classical electromagnetic theory, so there is no current monopole moment in general relativity. The current dipole moment $\mathcal{S}_1$ is the source's angular momentum J_k, so the leading-order term in the expansion (27.45) has the form (25.98c), which we have used to deduce the angular momenta of gravitating bodies.

If the source has mass M, size L and internal velocities $\sim v$, then the magnitudes of its moments are

$$\mathcal{I}_\ell \sim ML^\ell \,, \quad \mathcal{S}_\ell \sim MvL^\ell \tag{27.46}$$

These formulae guarantee that the near-zone fields g_{00} and g_{0j}, as given by Eqs. (27.44) and (27.45), are dimensionless.

As the source's moments oscillate dynamically, they produce gravitational waves. Mass-energy conservation [Eq. (25.102)] prevents the mass monopole moment $\mathcal{I}_0 = M$ from oscillating; angular-momentum conservation [Eq. (25.103)] prevents the current dipole moment $\mathcal{S}_1$ = (angular momentum) from oscillating; and because the time derivative of the mass dipole moment $\mathcal{I}_1$ is the source's linear momentum, momentum conservation [Eq. (25.106)] prevents the mass dipole moment from oscillating. Therefore, the lowest-order moments that can oscillate and thereby contribute to the waves are the quadrupolar ones. The wave fields h_+ and $h_\times$ in the source's local wave zone must (i) be dimensionless, (ii) die out as $1/r$, and (iii) be expressed as a sum over derivatives of the multipole moments. These considerations guarantee (Ex. 27.8) that the waves will have the following form:

$$\boxed{h_+ \sim h_\times \sim \frac{\partial^2 \mathcal{I}_2/\partial t^2}{r} \,\&\, \frac{\partial^3 \mathcal{I}_3/\partial t^3}{r} \,\&\, \ldots \,\&\, \frac{\partial^2 \mathcal{S}_2/\partial t^2}{r} \,\&\, \frac{\partial^3 \mathcal{S}_3/\partial t^3}{r} \,\&\, \ldots} \,. \tag{27.47}$$

The timescale on which the moments oscillate is $T \sim L/v$, so each time derivative produces a factor v/L. Correspondingly, the ℓ-pole contributions to the waves have magnitudes

$$\frac{\partial^\ell \mathcal{I}_\ell/\partial t^\ell}{r} \sim \frac{M}{r} v^\ell \,, \quad \frac{\partial^\ell \mathcal{S}_\ell/\partial t^\ell}{r} \sim \frac{M}{r} v^{(\ell+1)} \,. \tag{27.48}$$

This means that, for a *slow-motion source* (one with internal velocities v small compared to light so the reduced wavelength $\lambda\!\!\!^{-} \sim L/v$ is large compared to the source size L), *the mass quadrupole moment $\mathcal{I}_2$ will produce the strongest waves.* The mass octupole (3-pole) waves and current quadrupole waves will be weaker by $\sim v \sim L/\lambda\!\!\!^{-}$; the mass 4-pole and current octupole waves will be weaker by $\sim v^2 \sim L^2/\lambda\!\!\!^{-2}$, etc. This is analogous to the electromagnetic case, where the electric dipole waves are the strongest, the electric quadrupole and magnetic dipole are smaller by $\sim L/\lambda\!\!\!^{-}$, etc.

In the next section we shall develop the theory of mass-quadrupole gravitational waves. For the corresponding theory of higher-order multipoles, see, e.g., Blanchet (2014) and Sec. VIII of Thorne (1980).

****

EXERCISES

Exercise 27.8 *Derivation: Multipolar Expansion of Gravitational Waves*
Show that conditions (i), (ii) and (iii) preceeding Eq. (27.47) guarantee that the multipolar expansion of the gravitational-wave fields will have the form (27.47).

****

27.5.2 Quadrupole-moment formalism

Consider a weakly gravitating, nearly Newtonian system (which is guaranteed to be a slow-motion gravitational-wave source, since Newtonian theory requires internal velocities $v \ll 1$. An example is a binary star system. Write the system's Newtonian potential (in its near zone) in the usual way

$$\Phi(\mathbf{x}) = -\int \frac{\rho(\mathbf{x}')}{|\mathbf{x}-\mathbf{x}'|} d\mathcal{V}_{x'} \ . \tag{27.49}$$

By using Cartesian coordinates, placing the origin of coordinates at the center of mass so $\int \rho x^j d\mathcal{V}_x = 0$, and expanding

$$\frac{1}{|\mathbf{x}-\mathbf{x}'|} = \frac{1}{r} + \frac{x^j x^{j'}}{r^3} + \frac{x^j x^k (3x^{j'}x^{k'} - r'^2\delta_{jk})}{2r^5} + \dots \ , \tag{27.50}$$

we obtain the multipolar expansion of the Newtonian potential

$$\boxed{\Phi(\mathbf{x}) = -\frac{M}{r} - \frac{3\mathcal{I}_{jk}x^j x^k}{2r^5} + \dots} \ . \tag{27.51}$$

Here

$$\boxed{M = \int \rho d\mathcal{V}_x \ , \quad \mathcal{I}_{jk} = \int \rho \left(x^j x^k - \frac{1}{3} r^2 \delta_{jk} \right) d\mathcal{V}_x} \tag{27.52}$$

are the system's mass and mass quadrupole moment. Note that *the mass quadrupole moment is equal to the second moment of the mass distribution, with its trace removed.*

As we have discussed, dynamical oscillations of the quadrupole moment generate the source's strongest gravitational waves. Those waves must be describable, in the source's near zone and local wave zone, by an outgoing-wave solution to the Lorenz-gauge, linearized Einstein equations

$$\bar{h}_{\mu\nu,}{}^{\nu} = 0 \ , \quad \bar{h}_{\mu\nu,\alpha}{}^{\alpha} = 0 \tag{27.53}$$

[Eqs. (25.89) and (25.90)] that has the near-zone Newtonian limit

$$\frac{1}{2}(\bar{h}_{00} + \bar{h}_{xx} + \bar{h}_{yy} + \bar{h}_{zz}) = h_{00} = (\text{quadrupole part of } -2\Phi) = \frac{3\mathcal{I}_{jk}x^j x^k}{r} \tag{27.54}$$

[cf. Eq. (25.79)].

The desired solution can be written in the form

$$\boxed{\bar{h}_{00} = 2\left[\frac{\mathcal{I}_{jk}(t-r)}{r}\right]_{,jk}, \quad \bar{h}_{0j} = 2\left[\frac{\dot{\mathcal{I}}_{jk}(t-r)}{r}\right]_{,k}, \quad \bar{h}_{jk} = 2\frac{\ddot{\mathcal{I}}_{jk}(t-r)}{r}}, \tag{27.55}$$

where the coordinates are Cartesian, $r \equiv \sqrt{\delta_{jk}x^j x^k}$, and the dots denote time derivatives. To verify that this is the desired solution: (i) Compute its divergence $\bar{h}_{\alpha\beta,}{}^{\beta}$ and obtain zero almost trivially. (ii) Notice that each Lorentz-frame component of $\bar{h}_{\alpha\beta}$ has the form $f(t-r)/r$ aside from some derivatives that commute with the wave operator, which implies that it satisfies the wave equation. (iii) Notice that in the near zone, the slow-motion assumption inherent in the Newtonian limit makes the time derivatives negligible, so $\bar{h}_{jk} \simeq 0$ and $\bar{h}_{00}$ is twice the right-hand side of Eq. (27.54), as desired.

Because the trace-reversed metric perturbation (27.55) in the local wave zone has the speed-of-light-propagation form, aside from its very slow decay as $1/r$, we can compute the gravitational-wave field $h^{\rm TT}_{jk}$ from it by transverse-traceless projection, Eq. (3) of Box 27.2 with $\mathbf{n} = \mathbf{e}_r$:

$$\boxed{h^{\rm TT}_{jk} = 2\left[\frac{\ddot{\mathcal{I}}_{jk}(t-r)}{r}\right]^{\rm TT}}. \tag{27.56}$$

This is called *the quadrupole-moment formula for gravitational-wave generation*. Our derivation shows that it is valid for any nearly Newtonian source.

Looking back more carefully at the derivation, one can see that, in fact, it relied only on the linearized Einstein equations and the Newtonian potential in the source's local asymptotic rest frame. Therefore, *this quadrupole formula is also valid for slow-motion sources that have strong internal gravity (e.g., slowly spinning neutron stars), so long as we read the quadrupole moment $\mathcal{I}_{jk}(t-r)$ off the source's weak-field, near-zone Newtonian potential (27.51) and don't try to compute it via the Newtonian volume integral (27.52).*

When the source is nearly Newtonian, so the volume integral (27.52) can be used to compute the quadrupole moment, the computation of the waves is simplified by computing instead the second moment of the mass distribution

$$\boxed{I_{jk} = \int \rho x^j x^k d\mathcal{V}_x}, \tag{27.57}$$

which differs from the quadrupole moment solely in its trace. Then, because the TT projection is insensitive to the trace, the gravitational-wave field (27.56) can be computed as

$$\boxed{h^{\rm TT}_{jk} = 2\left[\frac{\ddot{I}_{jk}(t-r)}{r}\right]^{\rm TT}}. \tag{27.58}$$

27.5.3 Quadrupolar Wave Strength, Energy, Angular Momentum and Radiation Reaction

To get an order of magnitude feeling for the strength of the gravitational waves, notice that the second time derivative of the quadrupole moment, in order of magnitude, is the nonspherical part of the source's internal kinetic energy, $E^{\rm ns}_{\rm kin}$, so

$$\boxed{h_+ \sim h_\times \sim \frac{E^{\rm ns}_{\rm kin}}{r} = G\frac{E^{\rm ns}_{\rm kin}}{c^4 r}}, \tag{27.59}$$

where the second expression is written in conventional units. Although this estimate is based on the slow-motion assumption of source size small compared to reduced wavelength, $L \ll \lambda\!\!\!^{-}$, it remains valid in order of magnitude when extrapolated into the realm of the strongest of all realistic astrophysical sources, which have $L \sim \lambda\!\!\!^{-}$. In Ex. 27.16 we shall use Eq. (27.59) to estimate the strongest gravitational waves that might be seen by ground-based gravitational-wave detectors.

Because the gravitational stress-energy tensor $T^{\rm GW}_{\mu\nu}$ produces background curvature via the Einstein equation $G^{\rm B}_{\mu\nu} = 8\pi T^{\rm GW}_{\mu\nu}$, just like nongravitational stress-energy tensors, it must contribute to the rate of change of the source's mass M, linear momentum P_j and angular momentum J_i [Eqs. (25.102)–(25.106)] just like other stress-energies. When one inserts the quadrupolar $T^{\rm GW}_{\mu\nu}$ into Eqs. (25.102)–(25.106) and integrates over a sphere in the wave zone of the source's local asymptotic rest frame, one finds that (Ex. 27.11)

$$\boxed{\frac{dM}{dt} = -\frac{1}{5}\left\langle \frac{\partial^3 \mathcal{I}_{jk}}{\partial t^3}\frac{\partial^3 \mathcal{I}_{jk}}{\partial t^3}\right\rangle}, \tag{27.60}$$

$$\boxed{\frac{dJ_i}{dt} = -\frac{2}{5}\epsilon_{ijk}\left\langle \frac{\partial^2 \mathcal{I}_{jm}}{\partial t^2}\frac{\partial^3 \mathcal{I}_{km}}{\partial t^3}\right\rangle}, \tag{27.61}$$

and $dP_j/dt = 0$. It turns out [cf. Sec. IV of Thorne (1980)] that the dominant linear-momentum change (i.e., the dominant radiation-reaction "kick") arises from a beating of the mass quadrupole moment against the mass octupole moment, and mass quadrupole against current quadrupole:

$$\boxed{\frac{dP_i}{dt} = -\frac{2}{63}\left\langle \frac{\partial^3 \mathcal{I}_{jk}}{\partial t^3}\frac{\partial^4 \mathcal{I}_{jki}}{\partial t^4}\right\rangle - \frac{16}{45}\epsilon_{ijk}\left\langle \frac{\partial^3 \mathcal{I}_{jp}}{\partial t^3}\frac{\partial^3 \mathcal{S}_{kp}}{\partial t^3}\right\rangle}. \tag{27.62}$$

Here the mass octupole moment $\mathcal{I}_{jki}$ is the trace-free part of the third moment of the mass distribution, and the current quadrupole moment $\mathcal{S}_{kp}$ is the symmetric, trace-free part of the first moment of the vectorial angular momentum distribution. See, e.g., Secs. IV.C and V.C of Thorne (1980), or Sec. 3 of Thorne (1983).

The back reaction of the emitted waves on their source shows up not only in changes of the source's mass, momentum, and angular momentum, but also in accompanying changes of the source's internal structure. These structure changes can be deduced fully, in many cases, from dM/dt, dJ_j/dt and dP_j/dt. A nearly Newtonian binary system is an example (Sec.

27.5.4 below). However, in other cases (e.g., a compact body orbiting near the horizon of a massive black hole), the only way to compute the structure changes is via a *gravitational-radiation-reaction force* that acts back on the system.

The simplest example of such a force is one derived by William Burke (1971) for quadrupole waves emitted by a nearly Newtonian system. Burke's quadrupolar radiation-reaction force can be incorporated into Newtonian gravitation theory by simply augmenting the system's near-zone Newtonian potential with a radiation-reaction term, computed from the fifth time derivative of the system's quadrupole moment:

$$\boxed{\Phi^{\rm react} = \frac{1}{5}\frac{\partial^5 \mathcal{I}_{jk}}{\partial t^5} x^j x^k} \,. \tag{27.63}$$

This potential satisfies the vacuum Newtonian field equation $\nabla^2\Phi \equiv \delta_{jk}\Phi_{,jk} = 0$ because $\mathcal{I}_{jk}$ is trace free.

This augmentation onto the Newtonian potential arises as a result of general relativity's outgoing-wave condition. If one were to switch to an ingoing-wave condition, $\Phi^{\rm react}$ would change sign, and if the system's oscillating quadrupole moment were joined onto standing gravitational waves, $\Phi^{\rm react}$ would go away. In Ex. 27.12, it is shown that the radiation reaction force density $-\rho\boldsymbol{\nabla}\Phi^{\rm react}$ saps energy from the system at the same rate as the gravitational waves carry it away.

Burke's gravitational radiation-reaction potential $\Phi^{\rm react}$ and force density $-\rho\boldsymbol{\nabla}\Phi^{\rm react}$ are close analogs of the radiation reaction potential [last term in Eq. (16.79)] and acceleration [right side of Eq. (16.82)] that act on an oscillating ball that emits sound waves into a surrounding fluid. Moreover, Burke's derivation of his gravitational radiation-reaction potential is conceptually the same as the derivation, in Sec. 16.5.3, of the sound-wave reaction potential.

****

EXERCISES

Exercise 27.9 *Problem: Gravitational waves from arm waving*
Wave your arms rapidly, and thereby try to generate gravitational waves.

(a) Compute in order of magnitude, using classical general relativity, the wavelength of the waves you generate and their dimensionless amplitude at a distance of one wavelength away from you.

(b) How many gravitons do you produce per second? Discuss the implications of your result.

Exercise 27.10 *Example: Quadrupolar wave generation in linearized theory*
Derive the quadrupolar wave-generation formula (27.58) for a slow-motion, weak-gravity source in linearized theory, in Lorenz gauge, beginning with the retarded-integral formula

$$\bar{h}_{\mu\nu}(t,\mathbf{x}) = \int \frac{4T_{\mu\nu}(t-|\mathbf{x}-\mathbf{x}'|,\mathbf{x}'])}{|\mathbf{x}-\mathbf{x}'|} d\mathcal{V}_{x'} \tag{27.64}$$

[Eq. (25.91)]. Your derivation might proceed as follows:

(a) Show that for a slow-motion source, the retarded integral gives for the $1/r \equiv 1/|\mathbf{x}|$ (radiative) part of $\bar{h}_{jk}$

$$\bar{h}_{jk}(t,\mathbf{x}) = \frac{4}{r}\int T_{jk}(t-r,\mathbf{x}')d\mathcal{V}_{x'} \ . \tag{27.65}$$

(b) Show that in linearized theory in Lorenz gauge, the vacuum Einstein equations $-\bar{h}_{\mu\nu,\alpha}{}^{\alpha} = 16\pi T_{\mu\nu}$ [Eq. (25.90)] and the Lorenz gauge condition $\bar{h}_{\mu\nu,}{}^{\nu} = 0$ [Eq. (25.89)] together imply that the stress-energy tensor that generates the waves must have vanishing coordinate divergence, $T^{\mu\nu}{}_{,\nu} = 0$. This means that linearized theory is ignorant of the influence of self gravity on the gravitating $T^{\mu\nu}$!

(c) Show that this vanishing divergence implies $[T^{00}x^jx^k]_{,00} = [T^{lm}x^jx^k]_{,ml} - 2[T^{lj}x^k + T^{lk}x^j]_{,l} + 2T^{jk}$.

(d) By combining the results of (a) and (c), deduce that

$$\bar{h}_{jk}(t,\mathbf{x}) = \frac{2}{r}\frac{d^2I_{jk}(t-r)}{dt^2} \ , \tag{27.66}$$

where I_{jk} is the second moment of the source's (Newtonian) mass-energy distribution $T^{00} = \rho$ [Eq. (27.57)].

(e) Noticing that the trace-reversed metric perturbation (27.66) has the "speed-of-light-propagation" form, deduce that the gravitational-wave field $h^{\rm TT}_{jk}$ can be computed from (27.66) by a transverse-traceless projection, Box 27.2.

Comment: Part (b) shows that this linearized-theory analysis is incapable of deducing the gravitational waves emitted by a source whose dynamics is controlled by its self gravity, e.g., a nearly Newtonian binary star system. By contrast, the derivation of the quadrupole formula given in Sec. 27.5.2 is valid for any slow-motion source, regardless of the strength and roles of its internal gravity; see the discussion following Eq. (27.56).

Exercise 27.11 *Problem: Energy and Angular Momentum Carried by Gravitational Waves*

(a) Compute the net rate at which the quadrupolar waves (27.56) carry energy away from their source, by carrying out the surface integral (25.102) with T^{0j} being Isaacson's gravitational-wave energy flux (27.39). Your answer should be Eq. (27.60). [Hint: Perform the TT projection in Cartesian coordinates using the projection tensor, Eq. (2) of Box 27.2, and make use of the following integrals over solid angle on the unit sphere

$$\frac{1}{4\pi}\int n_i d\Omega = 0 \ , \quad \frac{1}{4\pi}\int n_in_j d\Omega = \frac{1}{3}\delta_{ij} \ , \quad \frac{1}{4\pi}\int n_in_jn_k d\Omega \ = 0; \ ,$$
$$\frac{1}{4\pi}\int n_in_jn_kn_l d\Omega = \frac{1}{15}(\delta_{ij}\delta_{kl} + \delta_{ik}\delta_{jl} + \delta_{il}\delta_{jk}). \tag{27.67}$$

These integrals should be obvious by symmetry, aside from the numerical factors out in front. Those factors are most easily deduced by computing the z components, i.e., by setting $i = j = k = l = z$ and using $n_z = \cos\theta$.]

(b) The computation of the waves' angular momentum can be carried out in the same way, but is somewhat delicate because a tiny nonradial component of the energy flux, that dies out as $1/r^3$, gives rise to the $\mathcal{O}(1/r^2)$ angular momentum flux. See Sec. IV.D of Thorne (1980).

Exercise 27.12 *Problem: Energy removed by gravitational radiation reaction*
Burke's radiation-reaction potential (27.63) produces a force per unit volume $-\rho\boldsymbol{\nabla}\Phi^{\rm react}$ on its nearly Newtonian source. If we multiply this force per unit volume by the velocity $\mathbf{v} = d\mathbf{x}/dt$ of the source's material, we obtain thereby a rate of change of energy per unit volume. Correspondingly, the net rate of change of the system's mass-energy must be

$$\frac{dM}{dt} = -\int \rho\mathbf{v}\cdot\boldsymbol{\nabla}\Phi^{\rm react} d\mathcal{V}_x \ . \tag{27.68}$$

Show that, when averaged over a few gravitational-wave periods, this formula agrees with the rate of change of mass (27.60) that we derived in Ex. 27.11 by integrating the outgoing waves' energy flux.

****

27.5.4 Gravitational Waves from a Binary Star System

A very important application of the quadrupole formalism is to wave emission by a nearly Newtonian binary star system. Denote the stars by indices A and B and their masses by M_A and M_B, so their total and reduced mass are (as usual)

$$\boxed{M = M_A + M_B \ , \quad \mu = \frac{M_A M_B}{M}} \ ; \tag{27.69a}$$

and let the binary's orbit be circular, for simplicity, with separation a between the stars' centers of mass. Then Newtonian force balance dictates that the orbital angular velocity Ω is given by Kepler's law,

$$\boxed{\Omega = \sqrt{M/a^3}} \ , \tag{27.69b}$$

and the orbits of the two stars are

$$x_A = \frac{M_B}{M} a\cos\Omega t \ , \quad y_A = \frac{M_B}{M} a\sin\Omega t \ , \quad x_B = -\frac{M_A}{M} a\cos\Omega t \ , \quad y_B = -\frac{M_A}{M} a\sin\Omega t \ . \tag{27.69c}$$

The second moment of the mass distribution, Eq. (27.57), is $I_{jk} = M_A x_A^j x_A^k + M_B x_B^j x_B^k$. Inserting the stars' time-dependent positions (27.69c), we obtain as the only nonzero components

$$I_{xx} = \mu a^2\cos^2\Omega t \ , \quad I_{yy} = \mu a^2 \sin^2\Omega t \ , \quad I_{xy} = I_{yx} = \mu a^2 \cos\Omega t \sin\Omega t \ . \tag{27.69d}$$

Noting that $\cos^2\Omega t = \frac{1}{2}(1+\cos 2\Omega t)$, $\sin^2\Omega t = \frac{1}{2}(1-\cos 2\Omega t)$ and $\cos\Omega t \sin\Omega t = \frac{1}{2}\sin 2\Omega t$, and evaluating the double time derivative, we obtain

$$\begin{aligned} \ddot{I}_{xx} &= -2\mu(M\Omega)^{2/3}\cos 2\Omega t\,, \quad \ddot{I}_{yy} = 2\mu(M\Omega)^{2/3}\cos 2\Omega t\,, \\ \ddot{I}_{xy} &= \ddot{I}_{yx} = -2\mu(M\Omega)^{2/3}\sin 2\Omega t\,. \end{aligned} \tag{27.69e}$$

We express this in terms of Ω rather than a because Ω is a direct gravitational-wave observable: the waves' angular frequency is 2Ω.

To compute the gravitational-wave field (27.56), we must project out the transverse traceless part of this $\ddot{I}_{jk}$. The projection is most easily performed in an orthonormal spherical basis, since there the transverse part is just the projection into the plane spanned by $\vec{e}_{\hat{\theta}}$ and $\vec{e}_{\hat{\phi}}$, and the transverse-traceless part has components

$$(\ddot{I}_{\hat{\theta}\hat{\theta}})^{\rm TT} = -(\ddot{I}_{\hat{\phi}\hat{\phi}})^{\rm TT} = \frac{1}{2}(\ddot{I}_{\hat{\theta}\hat{\theta}} - \ddot{I}_{\hat{\phi}\hat{\phi}})\,, \quad (\ddot{I}_{\hat{\theta}\hat{\phi}})^{\rm TT} = \ddot{I}_{\hat{\theta}\hat{\phi}} \tag{27.69f}$$

[cf. Eq. (1) of Box 27.2]. Now, a little thought will save us much work: We need only compute these quantities at $\phi = 0$ (i.e., in the x-z plane), since their circular motion guarantees that their dependence on t and ϕ must be solely through the quantity $\Omega t - \phi$. At $\phi = 0$, $\vec{e}_{\hat{\theta}} = \vec{e}_x\cos\theta - \vec{e}_z\sin\theta$ and $\vec{e}_{\hat{\phi}} = \vec{e}_y$, so the only nonzero components of the transformation matrices from the Cartesian basis to the transverse part of the spherical basis are $L^x{}_{\hat{\theta}} = \cos\theta$, $L^z{}_{\hat{\theta}} = -\sin\theta$, $L^y{}_{\hat{\phi}} = 1$. Using this transformation matrix, we obtain, at $\phi = 0$, $\ddot{I}_{\hat{\theta}\hat{\theta}} = \ddot{I}_{xx}\cos^2\theta$, $\ddot{I}_{\hat{\phi}\hat{\phi}} = \ddot{I}_{yy}$, $\ddot{I}_{\hat{\theta}\hat{\phi}} = \ddot{I}_{xy}\cos\theta$. Inserting these and expressions (27.69e) into Eq. (27.69f), and setting $\Omega t \to \Omega t - \phi$ to make the formulae valid away from $\phi = 0$, we obtain

$$\begin{aligned} (\ddot{I}_{\hat{\theta}\hat{\theta}})^{\rm TT} &= -(\ddot{I}_{\hat{\phi}\hat{\phi}})^{\rm TT} = -(1+\cos^2\theta)\,\mu(M\Omega)^{2/3}\cos[2(\Omega t-\phi)]\,, \\ (\ddot{I}_{\hat{\theta}\hat{\phi}})^{\rm TT} &= +(\ddot{I}_{\hat{\phi}\hat{\theta}})^{\rm TT} = -2\cos\theta\,\mu(M\Omega)^{2/3}\sin[2(\Omega t-\phi)]\,. \end{aligned} \tag{27.69g}$$

The gravitational-wave field (27.58) is $2/r$ times this quantity evaluated at the retarded time $t - r$.

We shall make the conventional choice for the polarization tensors:

$$\boxed{\mathbf{e}^+ = (\vec{e}_{\hat{\theta}}\otimes\vec{e}_{\hat{\theta}} - \vec{e}_{\hat{\phi}}\otimes\vec{e}_{\hat{\phi}})\,, \quad \mathbf{e}^\times = (\vec{e}_{\hat{\theta}}\otimes\vec{e}_{\hat{\phi}} + \vec{e}_{\hat{\phi}}\otimes\vec{e}_{\hat{\theta}})}\;; \quad \boxed{\vec{e}_{\hat{\theta}} = \frac{1}{r}\frac{\partial}{\partial\theta}\,, \quad \vec{e}_{\hat{\phi}} = \frac{1}{r\sin\theta}\frac{\partial}{\partial\phi}}\,. \tag{27.70a}$$

Then Eqs. (27.58) and (27.69g) tell us that the gravitational-wave field is, in slot-naming index notation,

$$\boxed{h^{\rm TT}_{\mu\nu} = h_+ e^+_{\mu\nu} + h_\times e^\times_{\mu\nu}}\,, \tag{27.70b}$$

where

$$\boxed{h_+ = h^{\rm TT}_{\hat{\theta}\hat{\theta}} = \frac{2}{r}[\ddot{I}_{\hat{\theta}\hat{\theta}}(t-r)]^{\rm TT} = -2(1+\cos^2\theta)\,\frac{\mu(M\Omega)^{2/3}}{r}\cos[2(\Omega t - \Omega r - \phi)]}\,, \tag{27.70c}$$

$$\boxed{h_\times = h^{\rm TT}_{\hat{\theta}\hat{\phi}} = \frac{2}{r}[\ddot{I}_{\hat{\theta}\hat{\phi}}(t-r)]^{\rm TT} = -4\cos\theta\,\frac{\mu(M\Omega)^{2/3}}{r}\sin[2(\Omega t - \Omega r - \phi)]}\,. \tag{27.70d}$$

We have expressed the ampitudes of these waves in terms of the dimensionless quantity $(M\Omega)^{2/3} = M/a = v^2$, where v is the relative velocity of the two stars.

Notice that, as viewed from the polar axis $\theta = 0$, h_+ and $h_\times$ are identical except for a $\pi/2$ phase delay, which means that the net stretch-squeeze ellipse (the combination of those in Figs. 27.1 and 27.2) rotates with angular velocity Ω. This is the gravitational-wave variant of circular polarization and arises because the binary motion as viewed from the polar axis looks circular. By contrast, as viewed by an observer in the equatorial plane $\theta = \pi/2$, $h_\times$ vanishes, so the net stretch-squeeze ellipse just oscillates along the + axes and the waves have linear polarization. This is natural, since the orbital motion as viewed by an equatorial observer is just a linear, horizontal, back-and-forth oscillation. Notice also that *the gravitational-wave frequency is twice the orbital frequency*, i.e.

$$\boxed{f = 2\frac{\Omega}{2\pi} = \frac{\Omega}{\pi}} \,. \tag{27.71}$$

To compute, via Eqs. (27.60) and (27.61), the rate at which energy and angular momentum are lost from the binary, we need to know the double and triple time derivatives of its quadrupole moment $\mathcal{I}_{jk}$. The double time derivative is just $\ddot{I}_{jk}$ with its trace removed, but Eq. (27.69d) shows that $\ddot{I}_{jk}$ is already trace free so $\ddot{\mathcal{I}}_{jk} = \ddot{I}_{jk}$. Inserting Eq. (27.69d) for this quantity into Eqs. (27.60) and (27.61) and performing the average over a gravitational-wave period, we find that

$$\boxed{\frac{dM}{dt} = -\frac{32}{\pi}\frac{\mu^2}{M^2}(M\Omega)^{10/3} \,, \quad \frac{dJ_z}{dt} = -\frac{1}{\Omega}\frac{dM}{dt} \,, \quad \frac{dJ_x}{dt} = \frac{dJ_y}{dt} = 0} \,. \tag{27.72}$$

This loss of energy and angular momentum causes the binary to spiral inward, decreasing the stars' separation a and increasing their orbital angular velocity Ω. By comparing Eqs. (27.72) with the standard equations for the binary's orbital energy and angular momentum, $M -$ (sum of rest masses of stars) $= E = -\frac{1}{2}\mu M/a = -\frac{1}{2}\mu(M\Omega)^{2/3}$, and $J_z = \mu a^2\Omega = \mu(M\Omega)^{2/3}/\Omega$, we obtain an equation for $d\Omega/dt$ which we can integrate to give

$$\boxed{\Omega = \pi f = \left(\frac{5}{256}\frac{1}{\mu M^{2/3}}\frac{1}{t_o - t}\right)^{3/8}} \,. \tag{27.73}$$

Here t_o (an integration constant) is the time remaining until the two stars merge, if the stars are thought of as point masses so their surfaces do not collide sooner. This equation can be inverted to read off the time until merger as a function of gravitational-wave frequency.

These results for a binary's waves and radiation-reaction-induced inspiral are of great importance for gravitational-wave detection; see, e.g., Cutler and Thorne (2002), and Sathyaprakash and Schutz (2009).

****

EXERCISES

Exercise 27.13 *Problem: Gravitational waves emitted by a linear oscillator*

Consider a mass m attached to a spring so it oscillates along the z axis of a Cartesian coordinate system, moving along the world line $z = a\cos\Omega t$, $y = x = 0$. Use the quadrupole moment formalism to compute the gravitational waves $h_+(t, r, \theta, \phi)$ and $h_\times(t, r, \theta, \phi)$ emitted by this oscillator, with the polarization tensors chosen as in Eqs. (27.70a). Pattern your analysis after the computation of waves from a binary in Sec. 27.5.4 .

Exercise 27.14 *** Example: Propagation of a binary's waves through an expanding universe*

As we shall see in Chap. 28, the following line element is a possible model for the large-scale structure of our universe:

$$ds^2 = b^2[-d\eta^2 + d\chi^2 + \chi^2(d\theta^2 + \sin^2\theta d\phi^2)] \ , \quad \text{where} \quad b = b_o\eta^2 \tag{27.74}$$

and b_o is a constant with dimensions of length. This is an expanding universe with flat spatial slices $\eta =$ constant. Notice that the proper time measured by observers at rest in the spatial coordinate system is $t = b_o \int \eta^2 d\eta = (b_o/3)\eta^3$.

A nearly Newtonian, circular binary is at rest at $\chi = 0$ in an epoch when $\eta \simeq \eta_o$. The coordinates of the binary's local asymptotic rest frame are (t, r, θ, ϕ), where $r = b\chi$ and the coordinates cover only a tiny region of the universe, $\chi \lesssim \chi_o \ll \eta_o$. The gravitational waves in this local asymptotic rest frame are described by Eqs. (27.70). Use geometric optics (Sec. 27.4.2) to propagate these waves out through the expanding universe. In particular:

(a) Show that the null rays along which the waves propagate are the curves of constant θ, ϕ, and $\eta - \chi$.

(b) Each ray can be characterized by the retarded time τ_r at which the source emitted it. Show that

$$\tau_r = \frac{1}{3} b_o (\eta - \chi)^3 \ . \tag{27.75a}$$

(c) Show that in the source's local asymptotic rest frame, this retarded time is $\tau_r = t - r$ and the phase of the wave is $\varphi = 2(\Omega\,\tau_r + \phi)$ [cf. Eqs. (27.70c) and (27.70d)]. Because the frequency Ω varies with time due to the binary inspiral, a more accurate formula for the wave's phase is $\varphi = 2(\int \Omega\, d\tau_r + \phi)$. Using Eq. (27.73), show that

$$\varphi = 2\phi - \left(\frac{t_o - \tau_r}{5\mathcal{M}}\right)^{5/8} \ , \quad \Omega = \frac{d\varphi}{d\tau_r} = \left(\frac{5}{256}\frac{1}{\mathcal{M}^{5/3}}\frac{1}{t_o - \tau_r}\right)^{3/8} \ , \tag{27.75b}$$

where

$$\mathcal{M} \equiv \mu^{3/5} M^{2/5} \tag{27.75c}$$

(with μ the reduced mass and M the total mass) is called the binary's *chirp mass* because, as Eqs. (27.75b) show, it controls the rate at which the binary's orbital angular frequency Ω and the gravitational-wave angular frequency 2Ω "chirp upward" as time passes. Since τ_r as given by Eq. (27.75a) is constant along rays when they travel out of the local wave zone and into and through the universe, so also: if we continue to write φ in terms of τ_r on those rays using Eq. (27.75b), this φ will be conserved along the rays in the external universe and therefore will satisfy the geometric optics equation $\nabla_{\vec{k}}\,\varphi = 0$ [Eq. (27.34b)].

(d) Show that the orthonormal basis vectors and polarization tensors

$$\vec{e}_{\hat{\theta}} = \frac{1}{b\chi}\frac{\partial}{\partial\theta}\ , \quad \vec{e}_{\hat{\phi}} = \frac{1}{b\chi\sin\theta}\frac{\partial}{\partial\phi}\ , \quad \mathbf{e}^{+} = (\vec{e}_{\hat{\theta}}\otimes\vec{e}_{\hat{\theta}} - \vec{e}_{\hat{\phi}}\otimes\vec{e}_{\hat{\phi}})\ , \quad \mathbf{e}^{\times} = (\vec{e}_{\hat{\theta}}\otimes\vec{e}_{\hat{\phi}} + \vec{e}_{\hat{\phi}}\otimes\vec{e}_{\hat{\theta}}) \tag{27.75d}$$

in the external universe: (i) are parallel transported along rays, and (ii) when carried backward on rays into the local asymptotic rest frame, become the basis vectors and tensors used in that frame's solution (27.70) for the gravitational waves. Therefore, these $e^{+}_{\mu\nu}$ and $e^{\times}_{\mu\nu}$ are the polarization tensors needed for our geometric optics waves.

(e) Consider a bundle of rays that, at the source, extends from ϕ to $\phi+\Delta\phi$ and from θ to $\theta+\Delta\theta$. Show that this bundle's cross sectional area, as it moves outward to larger and larger χ, is $\mathcal{A} = r^2\sin\theta\Delta\theta\Delta\phi$, where r is a function of η and χ given by

$$r = b\chi = b_o\eta^2\chi\ . \tag{27.75e}$$

Show that in the source's local asymptotic rest frame, this r is the same as the distance r from the source that appears in Eqs. (27.70c) and (27.70d) for h_+ and $h_\times$.

(f) By putting together all the pieces from parts (a) through (e), show that the solution to the equations of geometric optics (27.70) for the gravitational-wave field, as it travels outward through the universe is

$$\boldsymbol{h}^{\rm TT} = h_+\mathbf{e}^{+} + h_\times\mathbf{e}^{\times}\ , \tag{27.75f}$$

with $\mathbf{e}^{+}$ and $\mathbf{e}^{\times}$ given by Eqs. (27.75d), with h_+ and $h_\times$ given by

$$h_+ = -2(1+\cos^2\theta)\frac{\mathcal{M}^{5/3}\Omega^{2/3}}{r}\cos\varphi\ , \quad h_\times = -4\cos\theta\frac{\mathcal{M}^{5/3}\Omega^{2/3}}{r}\sin\varphi\ , \tag{27.75g}$$

and with Ω, φ and r given by Eqs. (27.75b), (27.75a) and (27.75e). [Hint: Note that all quantities in this solution except r are constant along rays, and r varies as $1/\sqrt{\mathcal{A}}$, where $\mathcal{A}$ is the area of a bundle of rays.]

(g) The angular frequency of the waves that are emitted at retarded time τ_r is $\omega_e = 2\Omega$. When received at earth these waves have a cosmologically redshifted frequency $\omega_r = \partial\varphi/\partial t$, where $t = (b_o/3)\eta^3$ is proper time measured at earth, and in the derivative we must hold fixed the spatial coordinates of the earth: $\{\chi,\theta,\phi\}$. The ratio of these frequencies is $\omega_e/\omega_r = 1+z$, where z is the so-called cosmological redshift of the waves. Show that $1+z = (\partial\tau_r/\partial t)^{-1} = \eta^2/(\eta-\chi)^2$.

(h) Show that the information carried by the binary's waves is the following: (i) From the ratio of the amplitudes of the two polarizations one can read off the inclination angle θ of the binary's spin axis to the line of signt to the binary. (ii) From the waves' measured angular frequency ω and its time rate of change $d\omega/dt$, one can read off $(1+z)\mathcal{M}$, the binary's redshifted chirp mass. (iii) From the amplitude of the waves, with θ and $(1+z)\mathcal{M}$ known, one can read off $(1+z)r$, a quantity known to cosmologists as the binary's *luminosity distance*. [Note: It is remarkable that gravitational

waves by themselves reveal the source's luminosity distance but not its redshift, while electromagnetic observations reveal the redshift but not the luminosity distance. This complementarity illustrates the importance and power of combined gravitational-wave and electromagnetic observations.]

****

27.5.5 T2 Gravitational Waves from Binaries Made of Black Holes and/or Neutron Stars: Numerical Relativity

Perhaps the most interesting sources of gravitational waves are binary systems made of two black holes, a black hole and a neutron star, or two neutron stars — so-called *compact binaries*. When the two bodies are far apart, their motion and waves can be described accurately by Newtonian gravity and the quadrupole-moment formalism: the formulas in Sec. 27.5.4. As the bodies spiral inward, $(M\Omega)^{2/3} = M/a = v^2$ grows larger, h_+ and $h_\times$ grow larger, and relativistic corrections to our Newtonian, quadrupole analysis grow larger. Those relativistic corrections (including current-quadrupole waves, mass-octupole waves, etc.) can be computed using a *post-Newtonian* expansion of the Einstein field equations, i.e. an expansion in $M/a \sim v^2$. The accuracies of ground-based detectors such as LIGO require that, for compact binaries, the expansion be carried at least to order v^7 beyond our Newtonian, quadrupole analysis! (Blanchet 2014).

At the end of the inspiral, the binary's bodies come crashing together. To compute the waves from this final merger, with an accuracy comparable to the expected observations, it is necessary to solve the Einstein field equation on a computer. The techniques for this are called *numerical relativity* (Baumgarte and Shapiro 2010).

For binary black holes with approximately equal masses, simulations using numerical relativity reveal that the total energy radiated in gravitational waves is $\Delta E \sim 0.1Mc^2$ where M is the binary's total mass. Most of this energy is emitted in the last ~ 5 to 10 cycles of waves, at wave periods $P \sim$ (10 to 20)GM/c^3 [i.e. frequencies $f = 1/P \sim$ 1000Hz$(10M_\odot/M)$]. The gravitational-wave power output in these last 5 to 10 cycles is $dE/dt \sim 0.1Mc^2/(100GM/c^3) = 0.001c^5/G$, which is roughly 10^{24} times the luminosity of the sun, and $10,000$ times the luminosity of all the stars in the universe put together! If the holes have masses $\sim 10M_\odot$, this enormous luminosity lasts for only ~ 0.1s and the total energy emitted is the rest-mass energy of the sun. If the holes have masses $\sim 10^9 M_\odot$, the enormous luminosity lasts for ~ 1 year, and the energy emitted is the rest-mass energy of 10^8 sun.

For the simplest case of two identical, nonspinning black holes that spiral together in a circular orbit, both waveforms (both wave shapes) have the simple time evolution shown in Fig. 27.6. As the holes spiral together, their amplitude and phase increase in accord with the Newtonian-quadrupole formulas (27.70) and (27.71), but by the time of this figure, post-Newtonian corrections are producing noticeable differences from those formulas. When the holes merge, the gravitational-wave amplitude reaches a maximum amplitude. The merged hole then vibrates and the waves "ring down" with exponentially decaying amplitude.

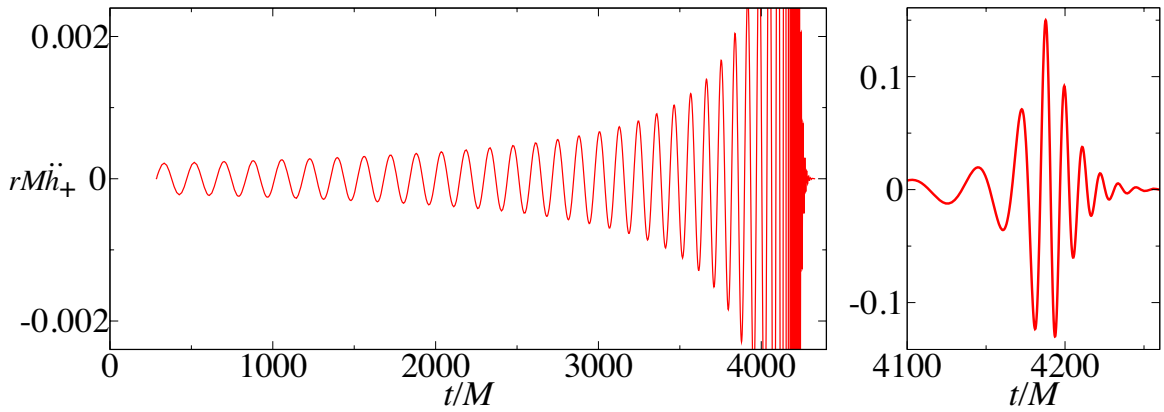

Fig. 27.6: For a binary made of two identical, nonspinning black holes that spiral together and merge: the time evolution of the gravitational-wave tidal field $\mathcal{E}_{ij} \propto \ddot{h}_+$ [Eq. (27.21)] for the + polarization. The other, × polarization waveform is the same as this, but with a phase shift. Based on simulations performed by the Caltech/Cornell/CITA numerical relativity group (Moroué et. al. 2013).

Much more interesting are binaries made of black holes that spin. In this case, the angular momentum of each spinning hole drags inertial frames, as does the binary's orbital angular momentum; this frame-dragging causes the spins and the orbital plane to precess; and those precessions modulate the waves. Figure 27.7 depicts a generic example: a binary whose holes have a mass ratio 6:1, dimensionless spins $a_A/M_A = 0.91$, $a_B/M_B = 0.30$, and randomly chosen initial spin axes and orbital plane. Frame dragging causes the orbital motion to be rather complex, and correspondingly the two waveforms are much richer than in the nonspinning case. The waveforms carry detailed information about the binary's masses, spins, and orbital evolution, and also about the geometrodynamics of its merger (Box 27.4).

****

EXERCISES

Exercise 27.15 ***T2*** *Problem: Maximum Gravitational-Wave Amplitude*
Extrapolating Eqs. (27.70)–(27.72) into the strong-gravity regime, estimate the maximum gravitational-wave amplitude and emitted power for a nonspinning binary black hole with equal masses, and with unequal masses. Compare with the results from numerical relativity discussed in the text.

****

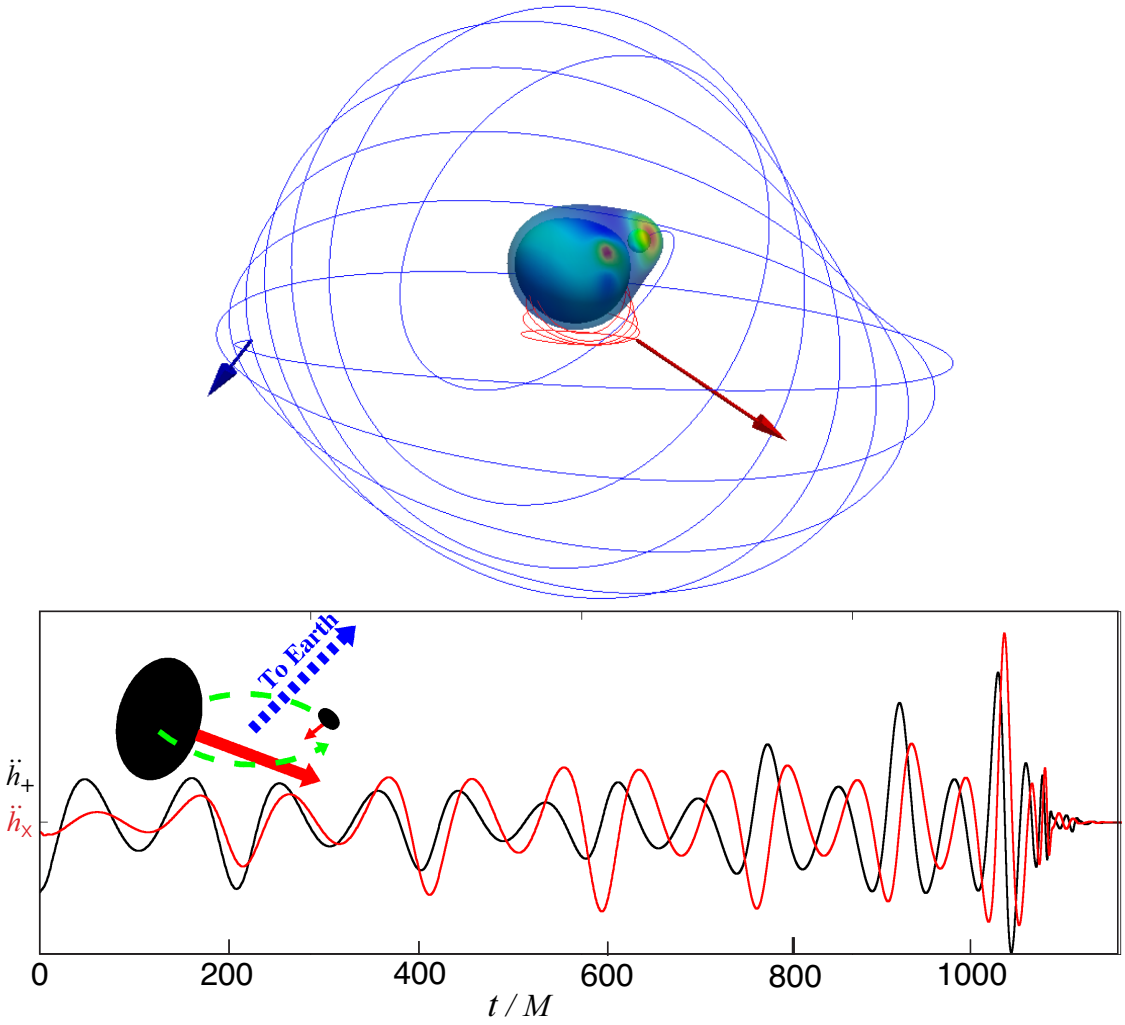

Fig. 27.7: Top panel: The orbital motion of a small black hole around a larger black hole (mass ratio $M_B/M_A = 1/6$), when the spins are $a_B/M_B = 0.30$ and $a_A/M_A = 0.91$ and the initial spin axes and orbital plane are as shown in the bottom panel. Bottom panel: the two gravitational waveforms emitted in the direction toward earth (blue dashed line). These waveforms are from a catalog of simulations of 174 different binary-black-hole mergers, carried out by the Caltech/Cornell/CITA numerical relativity group (Mroué et. al. 2013).

27.6 The Detection of Gravitational Waves

27.6.1 Frequency Bands and Detection Techniques

Physicists and astronomers are searching for gravitational waves in four different frequency bands using four different techniques:

- In the extremely low frequency (ELF) band, $\sim 10^{-15}$ to $\sim 10^{-18}$ Hz, gravitational waves are sought via their imprint on the polarization of the cosmic microwave background (CMB) radiation. There is only one expected ELF source of gravitational waves, but it is a very interesting one: quantum fluctuations in the gravitational field (spacetime

Box 27.4

T2 Geometrodynamics

When spinning black holes collide, they excite nonlinear vibrations of curved spacetime—a phenomenon that John Wheeler has called *geometrodynamics*. This nonlinear dynamics can be visualized using tidal tendex lines (which depict the tidal field $\mathcal{E}_{ij}$) and frame-drag vortex lines (which depict the frame-drag field $\mathcal{B}_{ij}$); see Boxes 25.2 and 26.3. Particularly helpful are the concepts of a *tendex* (a collection of tendex lines with large tendicities) and a *(frame-drag) vortex* (a collection of vortex lines with large vorticities). A spinning black hole has a counterclockwise vortex emerging from its north polar region, and a clockwise vortex emerging from its south polar region (lower right diagram in Box 26.3).

As an example of geometrodynamics, consider two identical black holes that collide head on, with their spins transverse to the collision direction. Numerical-relativity simulations (Owen et. al. 2011) reveal that, when the holes collide and merge, each hole deposits its two vortexes onto the merged horizon. The four vortexes dynamically attach onto each other in pairs [(a) below], and the pairs then interact, with surprising consequences:

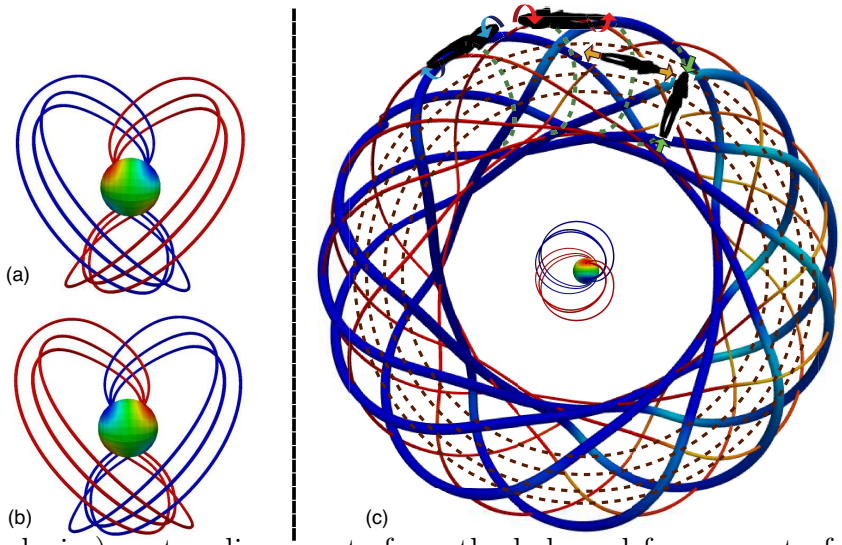

The blue (clockwise) vortex disconnects from the hole and forms a set of closed vortex loops that wrap around a torus [thick blue lines in (c)], and the red (counterclockwise) vortex does the same [thin red lines in (c)]. This torus expands outward at the speed of light, while energy temporarily stored in near-horizon tendexes (not shown) regenerates the new pair of horizon penetrating vortexes shown in (b), with reversed vorticities (reversed directions of twist). As the torus expands outward, its motion, via the Maxwell-like Bianchi identity $\partial\boldsymbol{\mathcal{E}}/\partial t = (\boldsymbol{\nabla}\times\boldsymbol{\mathcal{B}})^{\rm S}$ (Box 25.2), generates a set of tendex lines that wrap around the torus at 45-degree angles to the vortex lines [dashed lines in (c)]. The torus's interleaved vortex and tendex lines have become a gravitational wave, which locally looks like the plane wave discussed in Box 27.3. This process repeats, with amplitude damping, generating a sequence of expanding tori. [Figure adapted from Owen et. al. (2011).]

curvature) that emerge from the big bang's quantum-gravity regime, the *Planck era*, and that are subsequently amplified to classical, detectable sizes by the universe's early inflationary expansion. We shall study this amplification and the resulting ELF gravitational waves in Chap. 28 and shall see these waves' great potential for probing the physics of inflation.

- In the very low frequency (VLF) band, $\sim 10^{-7}$ to $\sim 10^{-9}$ Hz, gravitational waves are sought via their influence on the propagation of radio waves emitted by pulsars (spinning neutron stars) and by the resulting fluctuations in the arrival times of the pulsars' radio-wave pulses at earth (Ex. 27.19). The expected VLF sources are violent processes in the first fraction of a second of the universe's life (Chap. 28), and the orbital motion of extremely massive pairs of black holes in the distant universe.

- In the low frequency (LF) band, $\sim 10^{-4}$ to ~ 0.1 Hz, gravitational waves have been sought, in the past, via their influence on the radio signals by which NASA tracks interplanetary spacecraft. In the 2020s or 2030s, this technique will likely be supplanted by some variant of the proposed Laser Interferometer Space Antenna (LISA)—three "drag-free" spacecraft in a triangular configuration with 5-kilometer-long arms, that track each other via laser beams. LISA is likely to see waves from massive black-hole binaries (hole masses $\sim 10^5$ to $10^7 M_\odot$) out to cosmological distances; from small holes, neutron stars, and white dwarfs spiraling into massive black holes out to cosmological distances; from the orbital motion of white-dwarf binaries, neutron-star binaries, and stellar-mass black-hole binaries in our own galaxy; and possibly from violent processes in the very early universe.

- In the high frequency (HF) band, ~ 10 to $\sim 10^3$ Hz, is where earth-based detectors operate: laser interferometer gravitational-wave detectors such as LIGO, and resonant-mass detectors in which a gravitational wave alters the amplitude and phase of vibrations of a normal mode of a large, cylindrical bar. The interferometric detectors are likely to see waves from spinning, slightly deformed neutron stars (e.g. pulsars) in our Milky Way galaxy, and from a variety of sources in the more distant universe: the final inspiral and collisions of binaries made from neutron stars and/or stellar-mass black holes (up to hundreds of solar masses); the tearing apart of a neutron star by the spacetime curvature of a companion black hole; supernovae; the triggers of gamma ray bursts; and possibly waves from violent processes in the very early universe.

For detailed discussions of these gravitational-wave sources in all four frequency bands, and of prospects for their detection, see e.g. Cutler and Thorne (2002), Sathyaprakash and Schutz (2009), and references therein. It is likely that waves will be seen in all four bands by about 2030, and the first detection is likely to occur in the HF band before 2020, using the *Advanced LIGO* and possibly the *Advanced Virgo* gravitational-wave interferometers, with sensitivities $h_+ \sim h_\times \sim 10^{-22}$ near 100 Hz.

****

EXERCISES

Exercise 27.16 *Example: Strongest Gravitational Waves in High-Frequency Band*

(a) Using an order of magnitude analysis based on Eq. (27.59), show that the strongest gravitational waves that are likely to occur each year in LIGO's high-frequency band have $h_+ \sim h_\times \sim 10^{-21} - 10^{-22}$. [Hint: The highest nonspherical kinetic energy achievable must be for a highly deformed object (or two colliding objects), in which the internal velocities approach the speed of light — say, for realism, $v \sim 0.3c$. To achieve these velocities, the object's size L must be of order 2 or 3 Schwarzschild radii, $L \sim 5M$ where M is the source's total mass. The emitted waves must have $f \sim 0.01$ Hz (the frequency at the minimum of Advanced LIGO's noise curve—which is similar to initial LIGO, Fig. 6.7, but a factor ~ 10 lower). Using these considerations, estimate the internal angular frequency of the source's motion, and thence the source's mass, and thence the source's internal kinetic energy. Such a source will be very rare, so to see a few per year, its distance must be some substantial fraction of the Hubble distance. From this estimate $h_+ \sim h_\times$.]

(b) As a concrete example, estimate the gravitational-wave strength from the final moments of inspiral and merger of two black holes, as described by Eqs. (27.70) and (27.69b) extrapolated into the highly relativistic domain.

****

27.6.2 Gravitational-Wave Interferometers: Overview and Elementary Treatment

We briefly discussed earth-based gravitational-wave interferometers such as LIGO in Sec. 9.5, focusing on optical interferometry issues. In this chapter we shall analyze the interaction of a gravitational wave with such an interferometer. This analysis will not only teach us much about gravitational waves, but will also illustrate some central issues in the physical interpretation of general relativity theory.

To get quickly to the essentials, we shall examine a rather idealized interferometer: A Michelson interferometer (one without the input mirrors of Fig. 9.13) that floats freely in space, so there is no need to hang its mirrors by wires; see Fig. 27.8. In Sec. 27.6.5, we shall briefly discuss more realistic interferometers.

If we ignore delicate details, the operation of this idealized interferometer is very simple: As seen in a local Lorentz frame of the beam splitter, the gravitational wave changes the length of the x arm by $\delta x = \frac{1}{2} h_+ \ell_x$ where ℓ_x is the unperturbed length, and changes that of the y arm by the opposite amount $\delta y = -\frac{1}{2} h_+ \ell_y$ [Eqs. (27.28)]. The interferometer is operated with unperturbed lengths ℓ_x and ℓ_y that are nearly but not quite equal, so there is a small amount of light going toward the photodetector. The wave-induced change of arm length causes a relative phase shift of the light returning down the two arms to the beam splitter given by $\Delta\varphi(t) = \omega_o(2\delta y - 2\delta x) = \omega_o(\ell_x + \ell_y)h_+(t)$, where ω_o is the light's angular frequency (and we have set the speed of light to unity); cf. Sec. 9.5. This oscillating phase

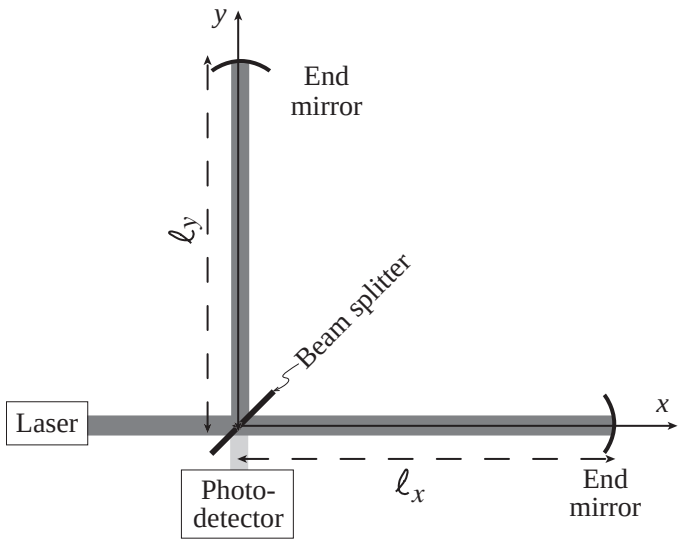

Fig. 27.8: An idealized gravitational-wave interferometer

shift modulates the intensity of the light going into the photodetector by $\Delta I_{\rm PD}(t) \propto \Delta\varphi(t)$. Setting $\ell_x \simeq \ell_y = \ell$, this modulation is

$$\boxed{\Delta I_{\rm PD}(t) \propto \Delta\varphi(t) = 2\omega_o \ell h_+(t)} \ . \tag{27.76}$$

Therefore, the photodetector output tells us directly the gravitational waveform $h_+(t)$.

In the following two (track-2) subsections, we shall rederive this result much more carefully in two different coordinate systems (two different gauges). Our two analyses will predict the same result (27.76) for the interferometer output, but they will appear to attribute that result to two different mechanisms.

In our first analysis (performed in TT gauge; Sec. 27.6.3), the interferometer's test masses will remain always at rest in our chosen coordinate system, and the gravitational waves $h_+(t-z)$ will interact with the interferometer's light. The imprint that $h_+(t-z)$ leaves on the light will cause a fluctuating light intensity $I_{\rm out}(t) \propto h_+(t)$ to emerge from the interferometer's output port and be measured by the photodetector.

In our second analysis (a more rigorous version of the above quick analysis, performed in the proper reference frame of the interferometer's beam splitter; Sec. 27.6.4) the gravitational waves will interact hardly at all with the light. Instead, they will push the end mirrors back and forth relative to the coordinate system, thereby lengthening one arm while shortening the other. These changing arm lengths will cause a changing interference of the light returning to the beam splitter from the two arms, and that changing interference will produce the fluctuating light intensity $I_{\rm out}(t) \propto h_+(t)$ measured by the photodetectors.

These differences of viewpoint are somewhat like the differences between the Heisenberg Picture and the Schrödinger Picture in quantum mechanics. The intuitive pictures associated with two viewpoints appear to be very different (Schrödinger's wave function vs. Heisenberg's matrices; gravitational waves interacting with light vs. gravitational waves pushing on mirrors). But whenever one computes the same physical observable from the

two different viewpoints (probability for a quantum measurement outcome; light intensity measured by photodetector), the two viewpoints give the same answer.

27.6.3 T2 Interferometer analyzed in TT gauge

For our first analysis, we place the interferometer at rest in the x-y plane of a TT coordinate system, with its arms along the x and y axes and its beam splitter at the origin as shown in Fig. 27.8 above. For simplicity, we assume that the gravitational wave propagates in the z direction and has + polarization, so the linearized spacetime metric has the TT-gauge form

$$\boxed{ds^2 = -dt^2 + [1 + h_+(t-z)]dx^2 + [1 - h_+(t-z)]dy^2 + dz^2} \tag{27.77}$$

[Eq. (27.19)]. For ease of notation, we shall omit the subscript + from h_+ in the remainder of this section.

The beam splitter and end mirrors move freely and thus travel along geodesics of the metric (27.77). The splitter and mirrors are at rest in the TT coordinate system before the wave arrives, so initially the spatial components of their 4-velocities vanish, $u_j = 0$. Because the metric coefficients $g_{\alpha\beta}$ are all independent of x and y, the geodesic equation dictates that the components u_x and u_y are conserved and thus remain zero as the wave passes, which implies (since the metric is diagonal) $u^x = dx/d\tau = 0$ and $u^y = dy/d\tau = 0$. One can also show (see Ex. 27.17) that $u^z = dz/d\tau = 0$ throughout the wave's passage. Thus, in terms of motion relative to the TT coordinate system, the gravitational wave has no influence at all on the beam splitter and mirrors; they all remain at rest (constant x, y and z) as the waves pass.

(Despite this lack of motion, the proper distances between the mirrors and the beam splitter—the interferometer's physically measured arm lengths—do change. If the unchanging coordinate lengths of the two arms are $\Delta x = \ell_x$ and $\Delta y = \ell_y$, then the metric (27.77) says that the physically measured arm lengths are

$$\boxed{L_x = \left[1 + \frac{1}{2}h(t)\right]\ell_x\ , \quad L_y = \left[1 - \frac{1}{2}h(t)\right]\ell_y}\ . \tag{27.78}$$

When h is positive, the x arm is lengthened and the y arm is shortened; when negative, L_x is shortened and L_y is lengthened.)

Turn, next, to the propagation of light in the interferometer. We assume, for simplicity, that the light beams have large enough transverse sizes that we can idealize them, on their optic axes, as plane electromagnetic waves. (In reality, they will be Gaussian beams, of the sort studied in Sec. 8.5.5). The light's vector potential A^α satisfies the curved-spacetime vacuum wave equation $A^{\alpha;\mu}{}_{\mu} = 0$ [Eq. (25.60) with vanishing Ricci tensor]. We write the vector potential in geometric optics (eikonal-approximation) form as

$$A^\alpha = \Re(\mathsf{A}^\alpha e^{i\varphi})\ , \tag{27.79}$$

where A^α is a slowly varying amplitude and φ is a rapidly varying phase; cf. Eq. (7.20). Because the wavefronts are (nearly) planar and the spacetime metric is nearly flat, the light's

amplitude A^α will be very nearly constant as it propagates down the arms, and we can ignore its variations. Not so the phase. It oscillates at the laser frequency $\omega_o/2\pi \sim 3\times 10^{14}$ Hz; i.e., $\varphi^{\rm out}_{x\ {\rm arm}} \simeq \omega_o(x-t)$ for light propagating outward from the beam splitter along the x arm, and similarly for the returning light and the light in the y arm. The gravitational wave places onto the phase tiny deviations from this $\omega_o(x-t)$; we must compute those deviations.

In the spirit of geometric optics, we introduce the light's spacetime wave vector

$$\vec{k} \equiv \vec{\nabla}\varphi \ , \tag{27.80}$$

and we assume that $\vec{k}$ varies extremely slowly compared to the variations of φ. Then the wave equation $A^{\alpha;\mu}{}_{\mu} = 0$ reduces to the statement that the wave vector is null, $\vec{k}\cdot\vec{k} = \varphi_{,\alpha}\varphi_{,\beta}g^{\alpha\beta} = 0$. For light in the x arm the phase depends only on x and t; for that in the y arm it depends only on y and t. Combining this with the TT metric (27.77) and noting that the interferometer lies in the $z=0$ plane, we obtain

$$\begin{aligned} -\left(\frac{\partial\varphi_{x\ {\rm arm}}}{\partial t}\right)^2 + [1-h(t)]\left(\frac{\partial\varphi_{x\ {\rm arm}}}{\partial x}\right)^2 &= 0 \ , \\ -\left(\frac{\partial\varphi_{y\ {\rm arm}}}{\partial t}\right)^2 + [1+h(t)]\left(\frac{\partial\varphi_{y\ {\rm arm}}}{\partial y}\right)^2 &= 0 \ . \end{aligned} \tag{27.81}$$

We idealize the laser as perfectly monochromatic and we place it at rest in our TT coordinates, arbitrarily close to the beam splitter. Then the outgoing light frequency, as measured by the beam splitter, must be precisely ω_o and cannot vary with time. Since proper time, as measured by the beam splitter, is equal to coordinate time t [cf. the metric (27.77))], the frequency that the laser and beam splitter measure must be $\omega = -\partial\varphi/\partial t = -k_t$. This dictates the following boundary conditions (initial conditions) on the phase of the light that travels outward from the beam splitter:

$$\frac{\partial\varphi^{\rm out}_{x\ {\rm arm}}}{\partial t} = -\omega_o \text{ at } x=0 \ , \quad \frac{\partial\varphi^{\rm out}_{y\ {\rm arm}}}{\partial t} = -\omega_o \text{ at } y=0 \ . \tag{27.82}$$

It is straightforward to verify that the solutions to Eq. (27.81) [and thence to the wave equation and thence to Maxwell's equations] that satisfy the boundary conditions (27.82) are

$$\begin{aligned} \varphi^{\rm out}_{x\ {\rm arm}} &= -\omega_o\left[t-x+\frac{1}{2}H(t-x)-\frac{1}{2}H(t)\right] \ , \\ \varphi^{\rm out}_{y\ {\rm arm}} &= -\omega_o\left[t-y-\frac{1}{2}H(t-y)+\frac{1}{2}H(t)\right] \ , \end{aligned} \tag{27.83}$$

where $H(t)$ is the first time integral of the gravitational waveform,

$$H(t) \equiv \int_0^t h(t')dt' \ ; \tag{27.84}$$

cf. Ex. 27.18.

The outgoing light reflects off the mirrors, which are at rest in the TT coordinates at locations $x = \ell_x$ and $y = \ell_y$. As measured by observers at rest in these coordinates, there is no doppler shift of the light because the mirrors are not moving. Correspondingly, the phases of the reflected light, returning back along the two arms, have the following forms:

$$\begin{aligned} \varphi^{\rm back}_{x\ {\rm arm}} &= -\omega_o \left[t + x - 2\ell_x + \frac{1}{2} H(t + x - 2\ell_x) - \frac{1}{2} H(t) \right] , \\ \varphi^{\rm back}_{y\ {\rm arm}} &= -\omega_o \left[t + y - 2\ell_y - \frac{1}{2} H(t + y - 2\ell_y) + \frac{1}{2} H(t) \right] . \end{aligned} \tag{27.85}$$

The difference of the phases of the returning light, at the beam splitter ($x = y = 0$), is

$$\begin{aligned} \Delta\varphi &\equiv \varphi^{\rm back}_{x\ {\rm arm}} - \varphi^{\rm back}_{y\ {\rm arm}} = -\omega_o [-2(\ell_x - \ell_y) + \frac{1}{2} H(t - 2\ell_x) + \frac{1}{2} H(t - 2\ell_y) - H(t)] \\ &\simeq +2\omega_o [\ell_x - \ell_y + \ell h(t)] \quad \text{for earth-based interferometers.} \end{aligned} \tag{27.86}$$

In the second line we have used the fact that for earth-based interferometers operating in the high-frequency band, the gravitational wavelength $\lambda_{\rm GW} \sim c/(100{\rm Hz}) \sim 3000$ km is long compared to the interferometers' ~ 4 km arms, and the arms have nearly the same length, $\ell_y \simeq \ell_x \equiv \ell$.

The beam splitter sends a light field $\propto e^{i\varphi^{\rm back}_{x\ {\rm arm}}} + e^{i\varphi^{\rm back}_{y\ {\rm arm}}}$ back toward the laser, and a field $\propto e^{i\varphi^{\rm back}_{x\ {\rm arm}}} - e^{i\varphi^{\rm back}_{y\ {\rm arm}}} = e^{i\varphi^{\rm back}_{y\ {\rm arm}}}(e^{i\Delta\varphi} - 1)$ toward the photodetector. The intensity of the light entering the photodetector is proportional to the squared amplitude of the field, $I_{\rm PD} \propto |e^{i\Delta\varphi} - 1|^2$. We adjust the interferometer's arm lengths so their difference $\ell_x - \ell_y$ is small compared to the light's reduced wavelength $1/\omega_o = c/\omega_o$ but large compared to $|\ell h(t)|$. Correspondingly, $|\Delta\varphi| \ll 1$, so only a tiny fraction of the light goes toward the photodetector (it is the interferometer's "dark port"), and that dark-port light intensity is

$$\boxed{I_{\rm PD} \propto |e^{i\Delta\varphi} - 1|^2 \simeq |\Delta\varphi|^2 \simeq 4\omega_o^2(\ell_x - \ell_y)^2 + 8\omega_o^2(\ell_x - \ell_y)\ell h_+(t)} . \tag{27.87}$$

Here we have restored the subscript + onto h. The time varying part of this intensity is proportional to the gravitational waveform $h_+(t)$ [in agreement with Eq. (27.76)], and it is this time varying part that the photodetector reports as the interferometer output.

****

EXERCISES

Exercise 27.17 ***T2*** *Derivation and Practice: Geodesic motion in TT coordinates*
Consider a particle that is at rest in the TT coordinate system of the gravitational-wave metric (27.77) before the gravitational wave arrives. In the text it is shown that the particle's 4-velocity has $u^x = u^y = 0$ as the wave passes. Show that $u^z = 0$ and $u^t = 1$ as the wave passes, so the components of the particle's 4-velocity are unaffected by the passing gravitational wave, and the particle remains at rest (constant x, y, and z) in the TT coordinate system.

Exercise 27.18 ***T2*** *Example: Light in an interferometric gravitational-wave detector in TT gauge*

Consider the light propagating outward from the beam splitter, along the x arm of an interferometric gravitational-wave detector, as analyzed in TT gauge, so (suppressing the subscript "x arm" and superscript "out") the electromagnetic vector potential is $A^\alpha = \Re(\mathsf{A}^\alpha e^{i\varphi(x,t)})$ with A^α constant and with $\varphi = -\omega_o\left[t - x + \frac{1}{2}H(t-x) - \frac{1}{2}H(t)\right]$ [Eqs. (27.83) and (27.84).]

(a) Show that this φ satisfies the nullness equation (27.81), as claimed in the text — which implies that $A^\alpha = \Re(\mathsf{A}^\alpha e^{i\varphi(x,t)})$ satisfies Maxwell's equations in the geometric optics limit.

(b) Show that this φ satisfies the initial condition (27.82), as claimed in the text.

(c) Show that, because the gradient $\vec{k} = \vec{\nabla}\varphi$ of this φ satisfies $\vec{k}\cdot\vec{k} = 0$, it also satisfies $\nabla_{\vec{k}}\vec{k} = 0$. Thus, the wave vector is the tangent vector to geometric optics rays that are null geodesics in the gravitational-wave metric. Photons travel along these null geodesics and have 4-momenta $\vec{p} = \hbar\vec{k}$.

(d) Because the gravitational-wave metric (27.77) is independent of x, the p_x component of a photon's 4-momentum must be conserved along its geodesic world line. Compute $p_x = k_x = \partial\varphi/\partial x$, and thereby verify this conservation law.

(e) Explain why the photon's frequency, as measured by observers at rest in our TT coordinate system, is $\omega = -k_t = -\partial\varphi/\partial t$. Explain why the rate of change of this frequency, as computed moving with the photon, is $d\omega/dt \simeq (\partial/\partial t + \partial/\partial x)\omega$, and show that $d\omega/dt \simeq -\frac{1}{2}\omega_o dh/dt$.

Exercise 27.19 ***T2*** *Example: Pulsar Timing Array*

An international collaboration of radio astronomers (IPTA 2013) is searching for gravitational waves by measuring the pulse arrival times for an array of pulsars spread over the sky—a Pulsar Timing Array, or PTA. Compute the influence of a planar gravitational wave on the arrival times, and discuss how the wave's direction and polarization can be read off the arrival-time data. More specifically:

(a) Introduce TT coordinates in which a pulsar is at rest at the origin and the earth also is at rest (for simplicity), at spatial location $x = \alpha L$, $y = \beta L$, $z = \gamma L$, with $\alpha^2 + \beta^2 + \gamma^2 = 1$. The linearized spacetime metric of the gravitational wave is Eq. (27.77), where for ease of notation we shall drop the + from h_+. Note from the metric that proper time, as measured by the pulsar and also on the earth, is equal to coordinate time t. Radio waves are emitted toward earth by the pulsar at its proper times $t_{\rm em} = 0,\ \tau,\ 2\tau,\ \ldots$ — i.e., with precisely constant interpulse spacings τ. Show that, to first order in h, the proper time $t_{\rm rec}$ that a pulse is received at earth differs from the proper time $t_{\rm em}$ it is emitted at the pulsar by

$$t_{\rm rec} - t_{\rm em} = L + \frac{\alpha^2 - \beta^2}{2}\int_0^L h(t_{\rm em} + [1-\gamma]r)dr\ . \tag{27.88}$$

Here the integral is with respect to distance r traveled by the pulse, from pulsar to earth.

[Hint: One way to derive this result is from the action $\frac{1}{2}\int g_{\alpha\beta}(dx^\alpha/d\zeta)(dx^\beta/d\zeta)d\zeta$ that underlies the rays' super-Hamiltonian; Ex. 25.7. The numerical value of the action is zero, and since it is an extremum along each true ray, if you evaluate it along a path that is a straight line in the TT coordinate system instead of along the true ray, you will still get zero at first order in h.]

(b) The arrival times of pulses at earth fluctuate, relative to their steady emission times, by some fractional amount $t'_{rec} \equiv dt_{\rm rec}/dt_{\rm em} - 1$ Show that

$$t'_{\rm rec} = \frac{(\alpha^2-\beta^2)(1+\gamma)}{\alpha^2+\beta^2}\left[h(t_{\rm rec}-\gamma L) - h(t_{\rm em})\right] \ . \tag{27.89}$$

Note that the first h is evaluated at the earth at the time of reception, and the second is evaluated at the pulsar at the time of emission. Thus, the fractional fluctuation of arrival times is proportional to the gravitational-wave field at reception minus that at emission, with a weighting factor that depends on the direction $\mathbf{n} = -\alpha\mathbf{e}_x - \beta\mathbf{e}_y - \gamma\mathbf{e}_z$ from the earth to the pulsar.

(c) The gravitational waves bathing the earth will produce correlated signals in the arrival-time fluctuations for the many pulsars in the PTA, while those bathing the pulsars at emission will not produce correlations, from pulsar to pulsar. Recognizing this, explain how the PTA data can be analyzed to extract the direction to and polarization of the gravitational waves from, say, a supermassive black-hole binary in some distant galaxy.

****

27.6.4 T2 Interferometer analyzed in the proper reference frame of the beam splitter

We now shall carefully reanalyze our idealized interferometer in the proper reference frame of its beam splitter, denoting that frame's coordinates by $\hat{x}^\alpha$. Because the beam splitter is freely falling (moving along a geodesic through the gravitational-wave spacetime), its proper reference frame is locally Lorentz ("LL"), and its metric coefficients have the form $g_{\hat\alpha\hat\beta} = \eta_{\alpha\beta} + {\rm O}(\delta_{jk}\hat{x}^j\hat{x}^k/\mathcal{R}^2)$ [Eq. (25.9a)]. Here $\mathcal{R}$ is the radius of curvature of spacetime, and $1/\mathcal{R}^2$ is of order the components of the Riemann tensor, which have magnitude $\ddot{h}(\hat{t}-\hat{z})$ [Eq. (27.21) with t and z equal to $\hat{t}$ and $\hat{z}$ aside from fractional corrections of order h]. Thus,

$$g_{\hat\alpha\hat\beta} = \eta_{\alpha\beta} + {\rm O}[\ddot{h}(\hat{t}-\hat{z})\delta_{jk}\hat{x}^j\hat{x}^k] \ . \tag{27.90}$$

(Here and below we again omit the subscript + on h for ease of notation.)

The following coordinate transformation takes us from the TT coordinates x^α used in the previous section to the beam splitter's LL coordinates:

$$x = \left[1 - \frac{1}{2}h(\hat{t}-\hat{z})\right]\hat{x}\ , \qquad y = \left[1 + \frac{1}{2}h(\hat{t}-\hat{z})\right]\hat{y}\ ,$$
$$t = \hat{t} - \frac{1}{4}\dot{h}(\hat{t}-\hat{z})(\hat{x}^2-\hat{y}^2)\ , \qquad z = \hat{z} - \frac{1}{4}\dot{h}(\hat{t}-\hat{z})(\hat{x}^2-\hat{y}^2)\ . \tag{27.91}$$

It is straightforward to insert this coordinate transformation into the TT-gauge metric (27.77) and thereby obtain, to linear order in h,

$$\boxed{ds^2 = -d\hat{t}^2 + d\hat{x}^2 + d\hat{y}^2 + d\hat{z}^2 + \frac{1}{2}(\hat{x}^2-\hat{y}^2)\ddot{h}(t-z)(d\hat{t}-d\hat{z})^2}\ . \tag{27.92}$$

This has the expected LL form (27.90) and, remarkably, it turns out not only to be a solution of the vacuum Einstein equations in linearized theory but also an exact solution to the full vacuum Einstein equations (cf. Ex. 35.8 of MTW)!

Throughout our idealized interferometer, the magnitude of the metric perturbation in these LL coordinates is $|h_{\hat{\alpha}\hat{\beta}}| \lesssim (\ell/\lambda\!\!\!^{-}_{\rm GW})^2 h$, where $\lambda\!\!\!^{-}_{\rm GW} = \lambda_{\rm GW}/2\pi$ is the waves' reduced wavelength and h is the magnitude of $h(\hat{t}-\hat{z})$. For earth-based interferometers operating in the HF band (~ 10 to ~ 1000 Hz), $\lambda\!\!\!^{-}_{\rm GW}$ is of order 50 to 5000 km, and the arm lengths are $\ell \leq 4$ km, so $(L/\lambda\!\!\!^{-})^2 \lesssim 10^{-2}$ to 10^{-6}. Thus, the metric coefficients $h_{\hat{\alpha}\hat{\beta}}$ are no larger than $h/100$. This has a valuable consequence for the analysis of the interferometer: Up to fractional accuracy $\sim (\ell/\lambda\!\!\!^{-}_{\rm GW})^2 h \lesssim h/100$, the LL coordinates are globally Lorentz throughout the interferometer; i.e., $\hat{t}$ measures proper time, and $\hat{x}^j$ are Cartesian and measure proper distance. In the rest of this section, we shall restrict attention to such earth-based interferometers, but shall continue to treat them as though they were freely falling. (See Sec. 27.6.5 for the influence of the earth's gravity.)

The beam splitter, being initially at rest at the origin of these LL coordinates, remains always at rest, but the mirrors move. Not surprisingly, the geodesic equation for the mirrors in the metric (27.92) dictates that their coordinate positions are, up to fractional errors of order $(\ell/\lambda\!\!\!^{-}_{\rm GW})^2 h$,

$$\hat{x} = L_x = \left[1 + \frac{1}{2}h(\hat{t})\right]\ell_x\ , \quad \hat{y} = \hat{z} = 0 \quad \text{for mirror in } x \text{ arm},$$
$$\hat{y} = L_y = \left[[1 - \frac{1}{2}h(\hat{t})\right]\ell_y\ , \quad \hat{x} = \hat{z} = 0 \quad \text{for mirror in } y \text{ arm}. \tag{27.93}$$

(This can also be deduced from the gravitational-wave tidal acceleration $-\mathcal{E}_{\hat{j}\hat{k}}\hat{x}^k$, as in Eq. (27.24), and from the fact that to good accuracy $\hat{x}$ and $\hat{y}$ measure proper distance from the beam splitter.) Thus, although the mirrors do not move in TT coordinates, they do move in LL coordinates. The two coordinate systems predict the same time-varying physical arm lengths (the same proper distances from beam splitter to mirrors), L_x and L_y [Eqs. (27.78) and (27.93)].

As in TT coordinates, so also in LL coordinates, we can analyze the light propagation in the geometric optics approximation, with $A^{\hat{\alpha}} = \Re(\mathcal{A}^{\hat{\alpha}} e^{i\varphi})$. Just as the wave equation

for the vector potential dictates, in TT coordinates, that the rapidly varying phase of the outward light in the x arm has the form $\varphi^{\rm out}_{x\ {\rm arm}} = -\omega_o(t-x) + {\rm O}(\omega_o \ell h_{\mu\nu})$ [Eq. (27.83) with $x \sim \ell \ll \lambda\!\!\!^{-}_{\rm GW}$ so $H(t-x) - H(t) \simeq \dot{H}(t)x = h(t)x \sim hL \sim h_{\mu\nu}L$], so similarly the wave equation in LL coordinates turns out to dictate that

$$\varphi^{\rm out}_{x\ {\rm arm}} = -\omega_o(\hat{t}-\hat{x}) + {\rm O}(\omega_o \ell h_{\hat{\mu}\hat{\nu}}) = -\omega_o(\hat{t}-\hat{x}) + {\rm O}\left(\omega_o \ell h \frac{\ell^2}{\lambda\!\!\!^{-2}_{\rm GW}}\right) \ , \tag{27.94}$$

and similarly for the returning light and the light in the y arm. The term ${\rm O}(\omega_o \ell h\ \ell^2/\lambda\!\!\!^{-2}_{\rm GW})$ is the influence of the direct interaction between the gravitational wave and the light. Aside from this term, the analysis of the interferometer proceeds in exactly the same way as in flat space (because $\hat{t}$ measures proper time and $\hat{x}$ and $\hat{y}$ proper distance): The light travels a round trip distance L_x in one arm and L_y in the other, and therefore acquires a phase difference, upon arriving back at the beam splitter, given by

$$\begin{aligned} \Delta\varphi &= -\omega_o[-2(L_x - L_y)] + {\rm O}\left(\omega_o \ell h \frac{\ell^2}{\lambda\!\!\!^{-2}_{\rm GW}}\right) \\ &\simeq +2\omega_o[\ell_x - \ell_y + \ell h(\hat{t})] + {\rm O}\left(\omega_o \ell h \frac{\ell^2}{\lambda\!\!\!^{-2}_{\rm GW}}\right) \ . \end{aligned} \tag{27.95}$$

This net phase difference for the light returning from the two arms is the same as we deduced in TT coordinates [Eq. (27.86)], up to the negligible correction ${\rm O}(\omega_o \ell h\ \ell^2/\lambda\!\!\!^{-2}_{\rm GW})$, and therefore the time-varying intensity of the light into the photodetector will be the same [Eq. (27.87)].

In our TT analysis the phase shift $2\omega_o \ell h(t)$ arose from the interaction of the light with the gravitational waves. In the LL analysis, it is due to the displacements of the mirrors in the LL coordinates (i.e., the displacements as measured in terms of proper distance), which cause the light to travel different distances in the two arms. The direct LL interaction of the waves with the light produces only the tiny correction ${\rm O}(\omega_o \ell h\ \ell^2/\lambda\!\!\!^{-2}_{\rm GW})$ to the phase shift.

It should be evident that the LL description is much closer to elementary physics than the TT description. This is always the case, when one's apparatus is sufficiently small that one can regard $\hat{t}$ as measuring proper time and $\hat{x}^j$ as Cartesian coordinates that measure proper distance throughout the apparatus. But for a large apparatus (e.g. planned space-based interferometers such as LISA, with arm lengths $\ell \gtrsim \lambda\!\!\!^{-}_{\rm GW}$) the LL analysis becomes quite complicated, as one must pay close attention to the ${\rm O}(\omega_o \ell h\ \ell^2/\lambda\!\!\!^{-2}_{\rm GW})$ corrections. In such a case, the TT analysis is much simpler.

27.6.5 T2 Realistic Interferometers

For realistic, earth-based interferometers, one must take account of the acceleration of gravity. Experimenters do this by hanging their beam splitters and test masses on wires or fibers. The simplest way to analyze such an interferometer is in the proper reference frame of the beam splitter, where the metric must now include the influence of the acceleration of gravity by adding a term $-2g\hat{z}$ to the metric coefficient $h_{\hat{0}\hat{0}}$ [cf. Eq. (24.60b)]. The resulting analysis, like that in the LL frame of our freely falling interferometer, will be identical to what one

would do in an accelerated reference frame of flat spacetime, so long as one takes account of the motion of the test masses driven by the gravitational-wave tidal acceleration $-\mathcal{E}_{\hat{i}\hat{j}}\hat{x}^j$, and so long as one is willing to ignore the tiny effects of $O(\omega_o \ell h\, \ell^2/\lambda\!\!\!^{-2}_{GW})$.

To make the realistic interferometer achieve high sensitivity, the experimenters introduce a lot of clever complications, such as the input mirrors of Fig. 9.13 which turn the arms into Fabry-Perot cavities. All these complications can be analyzed, in the beam splitter's proper reference frame, using standard flat-spacetime techniques augmented by the gravitational-wave tidal acceleration. The direct coupling of the light to the gravitational waves can be neglected, as in our idealized interferometer.

Bibliographic Note

For an elementary introduction to experimental tests of general relativity in the solar system, we recommend Chap. 10 of Hartle (2003). For an enjoyable, popular-level book on experimental tests, see Will (1993a). For a very complete monograph on the theory underlying experimental tests, see Will (1993b), and for a more nearly up to date review of experimental tests, see Will (2006).

For elementary and fairly complete introductions to gravitational waves, we recommend Chaps. 16 and 23 of Hartle (2003) and Chap. 9 of Schutz (2009). For more advanced treatments, we suggest Thorne (1983), Secs. 5.3–5.7 of Straumann (2013), and MTW Sec. 18.2 and Chaps. 35 and 36; but MTW Chap. 37 on gravitational-wave detection is terribly out of date and not recommended. For fairly complete reviews of gravitational-wave sources for ground-based detectors (LIGO etc.) and space-based detectors (LISA etc.), see Cutler and Thorne (2002) and Sathyaprakash and Schutz (2009). For a lovely monograph on the physics of interferometric gravitational-wave detectors, see Saulson (1994).

Because gravitational-wave science is a rapidly maturing and burgeoning field, there are long, in-depth treatments that include considerable experimental detail and much detail on data analysis techniques, as well as on wave sources and the fundamental theory: Maggiore (2008), Creighton and Anderson (2011), and Thorne, Bondarescu and chen (2002).

Bibliography

Baumgarte, T.W. and Shapiro, S.L., 2010. *Numerical Relativity: Solving Einstein's Equations on the Computer*, Cambridge: Cambridge University Press.

Bertotti, B., Iess, L. and Tortora, T., 2003. *Nature* **425**, 374.

Blanchet, L. 2014. "Gravitational radiation from Post-Newtonian sources and inspiraling compact binaries", *Living Reviews in Relativity*, in press; update of `http://www.livingreviews.org/lrr-2006-4`).

Burke, William L., 1971. "Gravitational radiation damping of slowly moving systems calculated using matched asymptotic expansions," *Journal of Mathematical Physics*, **12**, 402–418.

Box 27.5
Important Concepts in Chapter 27

- Experimental Tests of general relativity, Sec. 27.2
  - Weak equivalence principle (universality of free fall), Sec. 27.2.1
  - Gravitational redshift, Sec. 27.2.1
  - Perihelion shift, Sec.27.2.2 and Ex. 27.2
  - Fermat's principle, gravitational lenses, and deflection of light, Sec. 27.2.3 and Ex. 27.3
  - Shapiro time delay, Sec. 27.2.4
  - Frame dragging, Sec. 27.2.5
- Gravitational waves in flat spacetime, Sec. 27.3
  - Gravitational wave fields $\mathcal{E}_{ij}$, $h^{\rm TT}_{ij}$, h_+, $h_\times$ and their polarization tensors $\boldsymbol{e}^+$, $\boldsymbol{e}^\times$, Sec. 27.3.1
  - Computing $h^{\rm TT}_{ij}$, h_+, $h_\times$ from metric perturbation and its trace reversal $\bar{h}_{\alpha\beta}$ via TT projection, Box 27.2
  - Tidal forces and displacements produced by a gravitational wave, Sec. 27.3.2
  - Gravitons and their spin and rest mass, Sec. 27.3.3
  - Gravitational-wave stress-energy tensor, Sec. 27.4.3
- Gravitational waves propagating through a curved background spacetime, Sec. 27.4
  - Two-lengthscale definition of gravitational waves, Fig. 27.3
  - Gravitational wave equation, Eqs. (27.33)
  - Geometric optics propagation, Sec. 27.4.2
- Gravitational-wave generation, Sec. 27.5
  - Regions around a gravitational-wave source, Fig. 27.5
  - Multipolar expansion of h_+ and $h_\times$, Sec. 27.5.1
  - Slow-motion sources: quadrupole-moment formalism for computing wave generation, Sec. 27.5.2
  - Burke's radiation-reaction potential, Eq. (27.63)
  - Waves from a binary system, and binary inspiral, Sec. 27.5.4
- Gravitational-wave detection, Sec. 27.6
  - Frequency bands: ELF, VLF, LF and HF, Sec. 27.6
  - Interferometric gravitational-wave detector ("interferometer"), Sec. 27.6.3
  - How to analyze an interferometer in TT gauge (Sec. 27.6.3) and in the proper reference frame of the beam splitter (Sec. 27.6.4)

Ciufolini, Ignazio., Paolozzi, Antonio, Pavlis, Errios C., Ries, John, Koenig, Rolf, Matzner, Richard, Sindoni, Giampiero, and Neumayer, Hans 2011. "Testing Gravitational Physics with Stellite Laser Ranging", *European Physical Journal Plus* **126**, 72.

Cutler, Curt and Thorne, Kip S., 2002. "An overview of gravitational wave sources," in Proceedings of the GR16 Conference on General Relativity and Gravitation, ed. N. Bishop and S. D. Maharaj (World Scientific, 2002), 72–111; also available at http://xxx.lanl.gov/abs/gr-qc/0204090

Einstein, Albert, 1916. "Die Grundlage der allgemeinen Relativitätstheorie," *Annalen der Physik*, **49**, 769–822. English translation in Einstein *et al*. (1923).

Einstein, Albert, 1918. "Über Gravitationwellen," *Sitzungsberichte der Königlish Preussischen Akademie der Wissenschaften*, **1918 volume**, 154–167.

Everitt, C.W.F. et. al., 2011. "Gravity Probe B: Final Results of a Space Experiment to Test General Relativity", *Physical Review Letters*, **106**, 22101.

Fierz, Markus and Pauli, Wolfgang, 1939. "On relativistic wave equations for particles of arbitary spin in an electromagnetic field," *Proceedings of the Royal Society A*, **173**, 211–232.

Hartle, J. B., 2003. *Gravity: An Introduction to Einstein's General Relativity*, San Francisco: Addison-Wesley.

Iorio, Lorenzo, Ruggiero, Matteo Luca, and Corda, Christian 2013. "Novel Consideraitons about the Error Budget of the LAGEOS-Based Tests of Frame-Draggin with GRACE Geopotential Models", *Acta Astronautica* **91**, 141–148.

IPTA 2013. *International Pulsar Timing Array*, `http://www.ipta4gw.org`.

Isaacson, R. A. 1968a. "Gravitational Radiation in the Limit of High Frequency. I. The Linear Approximation and Geometrical Optics," *Physical Review* **166**, 1263–1271.

Isaacson, R. A. 1968b. "Gravitational Radiation in the Limit of High Frequency. II. Nonlinear Terms and the Effective Stress Tensor." *Physical Review* **166**, 1272–1280.

Merkowitz, Stephen M., 2010. "Tests of Gravity Using Lunar Laser Ranging", *Living Reviews in Relativity*, **13**, 7 (cited on 26 December 2013): `http://www.livingreviews.org/Irr-2010-7` .

MTW: Misner, Charles W., Thorne, Kip S. and Wheeler, John A., 1973. *Gravitation*, W. H. Freeman & Co., San Francisco.

Mroué, A. H. et. al. (the SXS Collaboration). 2013. "Catalog of 174 Binary Black HOle Simulations for Gravitational Wave Astronomy", *Physical Review Letters*, **111**, 241104.

Nichols, David et. al., 2012. "Visualizing Spacetime Curvature via Frame-Drag Vortexes and Tidal Tendexes: III. Quasinormal Pulsations of Schwarzschild and Kerr Black Holes," *Physical Review D*, submitted; `http://xxx.lanl.gov/pdf/1208.3038.pdf`.

Owen, R. et. al., 2011. "Frame-Dragging Vortexes and Tidal Tendexes Attached to Colliding Black Holes: Visualizing the Curvature of Spacetime," *Physical Review Letters*, **106**, 151101.

Sathyaprakash, B.S. and Schutz, B.F. 2009. "Physics, Astrophysics and Cosmology with Gravitational Waves", *Living Reviews in Relativity* **12**, 3 (cited on 26 December 2013): `http://www.livingreviews.org/Irr-2009-2` .

Saulson, Peter, *Fundamentals of Interferometric Gravitational Wave Detectors*, World Scientific, Singapore.

Schlamminger, S., Choi, K.-Y., Wagner, T.A., Gundlach, J.H., and Adelberger, E.G., 2008, "Test of the Equivalence Principle Using a Rotating Torsion Balance", *Physical Review Letters*, **100**, 041101.

Schutz, B. 2009. *A First Course in General Relativity*, second edition, Cambridge: Cambridge University Press

Stairs, I.H., 2010. "Binary Pulsars and Tests of General Relativity", in *Relativity in Fundamental Astronomy, Proceedings of IAU Symposium No. 261*, eds. S.A. Klioner P.K. Seidelman and M.H. Soffel, IAU Symposium Proceedings Series, **5**, 218–227.

Thorne, Kip S., 1980. *Review of Modern Physics*, **52**, 299.

Thorne, Kip S., 1983. "The Theory of Gravitational Radiation: An Introductory Review," in *Gravitational Radiation*, eds. N. Dereulle and T. Piran, North Holland, Amsterdam, pp. 1–57.

Thorne, Kip S., Bondarescu, Mihai and Chen, Yanbei, 2002. *Gravitational Waves: A Web-Based Course*, http://elmer.tapir.caltech.edu/ph237/

Weissberg, Joel M., Nice, David J. and Taylor, Joseph H. 2010. *Astrophysical Journal* **722**, 1030–.

Will, Clifford M., 1993a. *Was Einstein Right?: Putting General Relativity to the Test*, New York: Basic Books.

Will, Clifford M., 1993b. *Theory and Experiment in Gravitational Physics*, Revised Edition, Cambridge University press, Cambridge, UK.

Will, Clifford M., 2006. "The Confrontation between General Relativity and Experiment," *Living Reviews in Relativity* **9**, 3 (cited on 26 December 2013): `http://www.livingreviews.org/Irr-2006-3` .